

The sedentary survey of extreme high-energy peaked BL Lacs

III. Results from optical spectroscopy

S. Piranomonte¹, M. Perri², P. Giommi², H. Landt³, and P. Padovani⁴

¹ INAF, Osservatorio Astronomico di Roma, Via Frascati 33, 00040, Monte Porzio Catone (RM), Italy

² ASI Science Data Center, c/o ESA-ESRIN, via Galileo Galilei, I-00044 Frascati, Italy

³ Harvard-Smithsonian Center for Astrophysics, 60 Garden Street, MS-29 Cambridge, MA 02138, USA

⁴ European Southern Observatory, Karl-Schwarzschild-Str. 2, D-85748 Garching bei München, Germany

Received.. / Accepted...

ABSTRACT

Aims. The multi-frequency sedentary survey is a flux-limited, statistically well-defined sample of highly X-ray dominated (i.e., with a very high X-ray to radio flux ratio) BL Lacertae objects, which includes 150 sources. In this paper, the third of the series, we report the results of a dedicated optical spectroscopy campaign that, together with results from other independent optical follow-up programs, led to the spectroscopic identification of all sources in the sample.

Methods. We carried out a systematic spectroscopic campaign for the observation of all unidentified objects of the sample using the ESO 3.6m, the KPNO 4m, and the TNG optical telescopes.

Results. We present new identifications and optical spectra for 76 sources, 50 of which are new BL Lac objects, 18 are sources previously referred as BL Lacs but for which no redshift information was available, and 8 are broad emission-line AGNs. We find that the multi-frequency selection technique used to build the survey is highly efficient ($\sim 90\%$) in selecting BL Lacs objects. We present positional and spectroscopic information for all confirmed BL Lac objects. Our data allowed us to determine 36 redshifts out of the 50 new BL Lacs and 5 new redshifts for the previously known objects. The redshift distribution of the complete sample is presented and compared with that of other BL Lacs samples. For 26 sources without recognizable absorption features, we calculated lower limits to the redshift using a method based on simulated optical spectra with different ratios between jet and galaxy emission. For a subsample of 38 object with high-quality spectra, we find a correlation between the optical spectral slope, the 1.4 GHz radio luminosity, and the Ca H&K break value, indicating that for powerful/beamed sources the optical light is dominated by the non-thermal emission from the jet.

Key words. galaxies: active - galaxies: BL Lacertae surveys:

1. Introduction

BL Lacertae objects are strong radio-loud sources that constitute a rare subclass of active galactic nuclei (AGN) distinguished by peculiar and extreme properties, namely irregular and rapid variability, strong optical and radio polarization, lack of prominent emission lines, core-dominant radio morphology, and a broad continuum extending from the radio through high-energy γ -rays. Their broad-band spectra are characterized, in a νf_ν vs ν representation, by two emission peaks, the first located at IR/optical frequencies (but in several cases reaching the UV/X-ray band) and the second in the X-ray to γ -ray energy band. The physical process that is believed to produce the low energy peak is synchrotron emission from relativistic electrons in the jet, while inverse Compton scattering by the same population of relativistic electrons is thought to be at the origin of the higher energy peak (e.g., Ghisellini & Maraschi 1989). BL Lac objects are often divided into two classes according to the position of the synchrotron peak energy: low-energy peaked BL Lacs (LBLs), with the peak located at IR/optical wavelengths, and high-energy peaked BL Lacs (HBLs) with the synchrotron emission peaking in the UV/X-ray energy band (e.g., Giommi & Padovani 1994; Padovani & Giommi 1995a).

A still open issue is that of the evolutionary properties of BL Lacs. It has in fact been reported (e.g. Stickel et al. 1991; Morris et al. 1991) that BL Lacs have cosmological properties different from those of FSRQs and of all other type of AGNs. Although based on a few samples with rather small sizes, LBLs have been found to be consistent with being a non evolving population (Stickel et al. 1991), while HBLs seem to show a negative cosmological evolution; i.e. they are less numerous and/or less luminous at high redshift (Morris et al. 1991; Bade et al. 1998; Rector et al. 2000).

Because of these extreme physical characteristics and of their unusual cosmological evolution, BL Lacs have been the subject of intense research activity and observation campaigns from radio to TeV energies. HBLs are exceedingly rare with a density of less than one source (with radio flux larger than 3.5 mJy) every 100 square degrees (e.g., Giommi et al. 1999). A classical approach, which requires identifying all sources in a radio-flux limited survey, would only reveal one HBL every $\sim 10,000$ radio sources and would therefore be nearly impossible to pursue. All existing complete samples typically include less than 10 extreme HBLs, a subset far too small for any meaningful study.

The sedentary survey (Giommi, Menna, & Padovani 1999, hereafter referred to as Paper I) introduced a new multi-frequency, highly efficient approach to the discovery of HBLs. Using this method we have been able to assemble a well-defined,

radio-flux-limited, sample including 150 objects (Giommi et al. 2005, hereafter Paper II), which is currently the largest existing complete sample of high energy peaked BL Lacs.

In order to identify candidate BL Lacs in the sedentary survey, we carried out a large optical spectroscopic campaign during which we observed all the unidentified sources of the sample, therefore making the survey 100% spectroscopically identified. In this paper, we present new optical spectroscopic data for 76 objects obtained during several observing runs at the KPNO 4m, the ESO 3.6 m and the TNG 3.6 m telescopes.

The structure of the paper is as follows: in Section 2 we briefly describe the sedentary survey and its selection technique, Section 3 discusses the results of our optical spectroscopy, Section 4 reviews some of the sample properties, in particular the redshift distribution. Our conclusions are summarized in Section 5.

Throughout this paper we have assumed cosmological parameters $H_0 = 50 \text{ km s}^{-1} \text{ Mpc}^{-1}$ $q_0 = 0$. Spectral indices have been defined as $f_\nu \propto \nu^{-\alpha}$.

2. The sedentary survey

The Sedentary multi-frequency survey was designed to select a large and statistically well-defined sample of HBLs exploiting the fact that no other known source type has been found to possess such extreme spectral energy distribution. By imposing radio, optical, and X-ray flux ratios that are only consistent with the unique spectral energy distribution of HBL sources, it is then possible to statistically select large samples of these rare sources.

In the following we briefly recall the main definition criteria used to select this sample. We refer the reader to Papers I and II for details. The sample was extracted from a large set of radio and X-ray emitting sources obtained by cross-correlating the “ROSAT All Sky Survey Bright Source Catalog” (RASS-BSC) of soft (0.1-2 keV) X-ray sources (18,811 sources, Voges et al. 1999) with the NRAO VLA Sky Survey (NVSS) catalog of radio sources at 1.4 GHz (1,807,316 sources, Condon et al. 1998). Optical magnitudes of the sources have been obtained from Palomar and UK Schmidt surveys through the APM and COSMOS services (Irwin et al. 1994; Yentis et al. 1992).

The following conditions have been imposed in order to ensure that the sample is complete above a radio flux limit of $f_r \geq 3.5 \text{ mJy}$

1. $|b| > 20^\circ$;
2. $f_x/f_r \geq 3 \times 10^{-10} \text{ erg cm}^{-2} \text{ s}^{-1} \text{ Jy}^{-1}$;
3. $\alpha_{ro} > 0.2$;
4. $f_r \geq 3.5 \text{ mJy}$;
5. RASSBSC count rate $\geq 0.1 \text{ cts/s}$;
6. $V \leq 21$;

where α_{ro} is the usual broad-band spectral index between the radio (5GHz) and optical (5000 Å) fluxes, and V the visual apparent magnitude of the optical counterpart.

Condition 1) limits the survey area to high Galactic latitude regions where absorption due to Galactic N_H is low; condition 2) imposes a very high f_x/f_r flux ratio that, among radio loud sources, can be only reached by HBLs; condition 3) removes radio quiet sources from the sample, such as nearby Seyfert galaxies where the ratio between the unrelated radio and the X-ray flux accidentally satisfies condition 2); conditions 4) and 5) and 6) ensure statistical completeness above $f_r \geq 3.5 \text{ mJy}$.

The sample has also been updated to include a few new BL Lacs that happened to be just below the α_{ro} threshold of 0.2

used to separate BL Lacs from emission-line Seyfert galaxies (Giommi et al. 1999). In addition, a few spurious sources were found (consistent with the $\sim 15\%$ expected contamination from non BL Lac objects, Giommi et al. 1999) and removed from the sample.

Although the radio flux-limited sample was spectroscopically identified only at the $\sim 40\%$ level when the first results were published (1999), its content was expected to include a high fraction ($\sim 85\% - 90\%$) of HBL. This assumption is now confirmed both by the results of massive identification campaigns of X-ray sources discovered in the RASSBSC (Bauer et al. 2000; Schwope et al. 2000; Beckmann et al. 2003) and by our spectroscopic identification of the remaining unclassified objects.

The sedentary survey sample is now completely identified and includes 150 HBLs (see Paper II). The full catalog is presented in Paper II and it is also available on-line at <http://www.asdc.asi.it/sedentary/> where the broad-band spectral energy distributions and the optical finding charts are also provided.

3. Optical identification

The first identifications in the sample were obtained simply cross-correlating the precise NVSS positions with catalogs of known objects of different types. This first approach, discussed in Paper I, led to identification of 58 BL Lacs out of the original 155 HBL candidates.

In 1999 we started a systematic spectroscopic identification campaign to observe all the remaining HBL candidates or to obtain good-quality optical spectra of those objects already identified as BL Lacs but for which no redshift information was available. At the same time, Bauer et al. (2000) and Schwope et al. (2000) published the first results of the optical spectroscopic identification of bright X-ray sources in the ROSAT All Sky Survey, and Beckmann (2000) reports optical identification of part of the Hamburg-RASS bright X-ray AGN sample (later published in Beckmann et al. 2003). As expected, a significant fraction (about 40 objects) of the sedentary survey HBL candidates was found among these new classifications and thus the fraction of identified candidates in our sample significantly increased. In August 2003 our spectroscopic program was completed with the identification of all candidates leading to a final sample of 150 spectroscopically identified HBLs.

3.1. Spectroscopic observations

Spectroscopic observations of the Sedentary sources still unidentified and of BL Lacs without redshift were carried out during the period 1999–2003 at the KPNO 4 m, at the ESO 3.6m and at the TNG telescopes. The properties of grisms used in these runs are summarized in Table 1.

Finders of all the objects observed were taken from the on-line Digitized Sky Survey (DSS) in which both the X-ray and radio error circles have been plotted. This procedure is illustrated in Figs. 1 where it is shown that the accurate NVSS coordinate ($\leq 3''$) in most cases permits a firm identification of the optical counterpart to be obtained.

Follow-up observations were made of 76 objects, including the unidentified BL Lacs candidates (58) and objects already classified as BL Lac from literature but without a redshift determination (18). In total we discovered 50 new BL Lac objects, according to the classification criteria employed in the classification scheme of Marchã et al. (1996); additionally, we determined

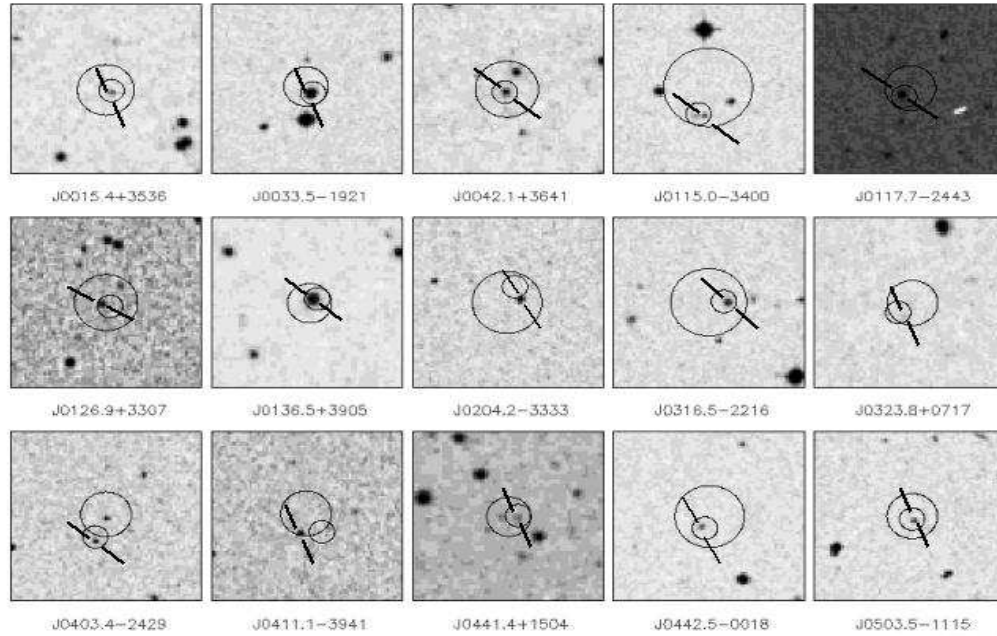


Fig. 1. A sample of optical finding charts of HBL sources observed by us. The X-ray and radio error circles (large and small, respectively) are shown.

Table 1. Grism properties

Telescope	Grism	Dispersion ($\text{\AA}/\text{pix}$)	Range (\AA)
TNG 3.6 m	LR-B Grism 1	2.8	3800–8000
ESO 3.6 m	Grism 1	6.66	3185–10940
	Grism 6	2.06	3860–8070
	Grism 13	2.77	3685–9315
KPNO 4 m	Grism 810	9.1	4300–10000

5 new redshifts out of 18 already known BL Lacs. The remaining 8 objects observed by us were broad emission-line AGN that were excluded from the sample (see Table 3 of Paper II).

Adding the identifications from the literature published in Giommi et al. (2005), our technique is $\sim 90\%$ efficient at selecting BL Lacs of the HBL type. In Table 2 we list the journal of observations for the 50 new BL Lacs discovered, for the 18 BL Lacs already known, and for the 8 broad emission lines AGNs. Columns are as follows: (1) name of the source, (2) telescope name, (3) date of observation, (4) exposure time (sec).

Standard data reduction was performed using different packages in IRAF¹ to obtain 1-dimensional wavelength-calibrated extracted spectra. The data were bias-subtracted and flat-fielded using programs in the IRAF package *noao.imred.ccdred*, and the spectra were extracted, wavelength-, and flux-calibrated using programs in the package *noao.twodspec*. A dereddening correction was applied to the data using the IRAF routine *noao.onedspec.deredden* and assuming Galactic values of extinction derived from 21-cm measurements (Stark et al. 1992).

¹ IRAF is distributed by the National Optical Astronomy Observatories, which are operated by the Association of the Universities for Research in Astronomy, Inc., under cooperative agreement with the National Science Foundation

The spectra were wavelength-calibrated using an He-Ar (ESO), He (TNG), or He-Ne-Ar (KPNO) reference spectrum. The photometric standard stars used for the relative flux calibration are: Hiltner600 (TNG 02/2002), HR1544 (TNG 02/2002, TNG 09/2002), LTT3864 (ESO 05/2003), BD3326 (TNG 02/2003, KPNO 02/1999), CD3299 (ESO 07/2001), and LTT7379 (ESO 08/2003).

In general, we took two exposures for each object (except in few cases for which we have only one spectrum) in order to combine them and improve the signal-to-noise ratio (S/N) if necessary; this procedure allowed us to remove bad pixels and spurious features and to check the reliability of detected absorption and/or emission lines. In some cases dead pixels and cosmic rays were removed manually.

Most of the spectra were taken at parallactic angle, except in those cases where the radio/X-ray error circle contained two candidates, so a rotation of the slit was necessary. In those cases (8 objects) where we found two objects in the NVSS error box, we took the spectra of both objects. We always found that one object was a BL Lac and the other a star.

3.2. Positional information

In Table 3 we list all the positional information, including the ones from RASSBSC and NVSS surveys, for the 76 sources observed during our identification campaign. These form, together with the previously known sources, the complete sample published in Paper II. Columns are as follows: (1) name of the source, (2) and (3) RASSBSC position, (4) and (5) NVSS position, (6) and (7) position of the optical counterpart, which is taken from the on-line services APM and COSMOS and confirmed by our observations.

Table 2. Log of observations

Name	Observatory	Date	Exp [sec]	Name	Observatory	Date	Exp [sec]
SHBL J001527.9+353639	TNG 3.6 m	2002 Sep	2400	SHBL J125015.5+315559	TNG 3.6 m	2002 Feb	3600
SHBL J003334.2-192133	ESO 3.6 m	2001 July	900	SHBL J125341.1-393159	ESO 3.6 m	2001 July	2400
SHBL J004208.0+364112	TNG 3.6 m	2002 Sep	2400	SHBL J140630.1-393509	ESO 3.6 m	2003 May	3600
SHBL J011501.9-340028	ESO 3.6 m	2003 Aug	3600	SHBL J140630.2+123620	ESO 3.6 m	2003 May	4800
SHBL J011747.0-244333	ESO 3.6 m	2001 July	2700	SHBL J140659.2+164207	ESO 3.6 m	2003 May	1200
SHBL J012657.2+330730	TNG 3.6 m	2002 Sep	2400	SHBL J142739.5-252102	ESO 3.6 m	2001 July	2700
SHBL J013632.5+390559	TNG 3.6 m	2002 Sep	600	SHBL J143917.4+393243	TNG 3.6 m	2003 Feb	2700
SHBL J020412.8-333342	ESO 3.6 m	2001 July	2400	SHBL J144506.3-032612	ESO 3.6 m	2003 May	2400
SHBL J031633.7-221611	ESO 3.6 m	2001 July	3000	SHBL J150340.6-154113	ESO 3.6 m	2001 July	1800
SHBL J032350.7+071736	ESO 3.6 m	2003 Aug	3600	SHBL J150637.0-054004	ESO 3.6 m	2003 May	2400
SHBL J040324.5-242950	ESO 3.6 m	2003 Aug	1800	SHBL J151041.0+333504	KPNO 4 m	1999 Feb	600
SHBL J041112.2-394143	ESO 3.6 m	2001 July	3600	SHBL J151618.6-152343	ESO 3.6 m	2003 May	1200
SHBL J044127.4+150456	ESO 3.6 m	2003 Aug	2400	SHBL J153311.3+185428	TNG 3.6 m	2002 Sep	2400
SHBL J044230.1-001830	TNG 3.6 m	2002 Sep	1800	SHBL J161204.6-043815	ESO 3.6 m	2000 Aug	2700
SHBL J050335.3-111507	TNG 3.6 m	2003 Feb	1800	SHBL J161632.9+375602	TNG 3.6 m	2002 Feb	1800
SHBL J050939.8-251403	ESO 3.6 m	2003 Aug	2400	SHBL J163658.4-124837	ESO 3.6 m	2001 July	3600
SHBL J060714.3-251859	ESO 3.6 m	2003 May	2400	SHBL J174702.3+493801	TNG 3.6 m	2002 Sep	3600
SHBL J062149.6-341149	ESO 3.6 m	2003 May	3600	SHBL J175615.9+552217	TNG 3.6 m	2002 Sep	2400
SHBL J075124.9+173051	KPNO 4 m	1999 Feb	600	SHBL J184822.3+653657	TNG 3.6 m	2002 Sep	1200
SHBL J075324.6+292132	TNG 3.6 m	2002 Feb	2400	SHBL J203844.8-263633	ESO 3.6 m	2001 July	2400
SHBL J092401.1+053345	TNG 3.6 m	2002 Feb	2400	SHBL J204735.8-290859	ESO 3.6 m	2001 July	2700
SHBL J094355.5-070951	ESO 3.6 m	2003 May	3600	SHBL J204921.7+003926	ESO 3.6 m	2000 Aug	1800
SHBL J095224.0+750213	KPNO 4 m	1999 Feb	1200	SHBL J205242.7+081038	TNG 3.6 m	2002 Sep	1800
SHBL J095805.9-031740	TNG 3.6 m	2002 Feb	3600	SHBL J213135.4-091523	ESO 3.6 m	2001 July	1200
SHBL J101015.9-311908	ESO 3.6 m	2003 May	1200	SHBL J213151.3-251558	ESO 3.6 m	2001 July	1800
SHBL J102243.8-011302	ESO 3.6 m	2003 May	2400	SHBL J213852.5-205348	ESO 3.6 m	2000 Aug	1800
SHBL J104651.4-253545	ESO 3.6 m	2003 May	1200	SHBL J222253.8-175321	ESO 3.6 m	2003 May	2400
SHBL J111939.5-304720	ESO 3.6 m	2003 May	3600	SHBL J224910.7-130002	ESO 3.6 m	2001 July	2700
SHBL J113444.5-172902	ESO 3.6 m	2003 May	3600	SHBL J225147.3-320614	ESO 3.6 m	2001 July	2700
SHBL J113755.4-171042	ESO 3.6 m	2003 May	3600	SHBL J230436.8+370507	TNG 3.6 m	2002 Sep	2400
SHBL J114535.1-034001	TNG 3.6 m	2003 Feb	3600	SHBL J230722.0-120518	ESO 3.6 m	2003 May	2400
SHBL J123417.1-385635	ESO 3.6 m	2001 July	2400	SHBL J231028.0-371909	ESO 3.6 m	2001 July	2400
SHBL J123511.0-140322	ESO 3.6 m	1999 Mar	1800	SHBL J234333.8+344004	TNG 3.6 m	2002 Sep	3600
SHBL J124149.3-145558	ESO 3.6 m	2003 May	1200	SHBL J235023.2-243603	ESO 3.6 m	2001 July	1200
1RXS J023727.6-26302	ESO 3.6 m	2001 July	2400	1RXS J170817.7-03493	ESO 3.6 m	1999 Mar	1800
1RXS J123802.1+36164	TNG 3.6 m	2002 Feb	2400	1RXS J182042.7+38171	TNG 3.6 m	2002 Sep	2400
1RXS J130350.5-39503	ESO 3.6 m	2001 Jul	2400	1RXS J212516.7-25553	ESO 3.6 m	2000 Aug	1800
1RXS J133950.5+15593	KPNO 4 m	1999 Feb	1200	1RXS J222944.5-27553	ESO 3.6 m	2001 July	2400

3.3. Optical spectra

In Appendix A, we present the spectra of the optical counterparts of all BL Lacs observed by us (68). In Appendix B, for completeness, we also present the spectra of the 8 AGNs with emission lines excluded from the sample. All spectra were smoothed with a Gaussian filter of 3 pixel width.

The complete list of the observed BL Lacs objects (the 18 BL Lacs already known are marked with *d*), together with their properties, are given in Table 4, where the columns are as follows: (1) source name, (2) unabsorbed 0.1 – 2.4 keV X-ray flux; (3) NVSS radio flux at 6 cm; (4) *V* magnitude estimated from *O* and *E* magnitudes obtained from the APM for the northern hemisphere and from the COSMOS *B_J* magnitudes as given in Paper I; (5) redshift, computed, whenever possible, by taking the mean of the consistent values derived from the absorption features; and (6) optical spectral slope between the rest frame frequencies of [*O II*] $\lambda 3727$ and [*O III*] $\lambda 5007$. The Ca H&K break value *C* is given in column (7) and was measured in spectra f_{λ} versus λ following (Dressler & Shectman 1987) as $C = 1 - f_{-}/f_{+}$, where f_{-} and f_{+} are the fluxes in the rest frame wavelength regions 3750 – 3950 Å and 4050 – 4250 Å, respectively. We have considered the Ca H&K break to have reached its minimum value of zero when $f_{-} \geq f_{+}$. Its 1 σ error was calculated based on the S/N

blueward and redward of this feature. Finally, in column (8) we give the average S/N of the spectrum around 5500 Å measured in several ~ 200 Å intervals and in (9) the 2 σ upper limits on observed emission-line equivalent widths are shown. For the latter we have assumed a rectangular emission line of $FWHM = 2000$ km/s centered at 5500 Å.

3.4. Redshift determination

In the optical band, the spectrum of a BL Lac is made up of two main components: (i) the amplified non-thermal jet emission, which follows a power-law of the form $f_{\nu} \propto \nu^{-\alpha}$, with α the spectral index, and (ii) thermal emission from the host galaxy, normally a luminous elliptical (e.g., Wurtz et al. 1996; Urry et al. 2000). The emission-line regions in BL Lacs are, by definition, only very weak or absent (see Section 3.5. for more details), which means that their redshift determination relies strongly on the detection of galaxy absorption features. This, however, is only possible if the jet is weak relative to the galaxy, i.e., only for low-luminosity BL Lacs. In strongly beamed sources, the jet with its featureless spectrum will dilute any galaxy absorption features beyond recognition (Landt, Padovani, & Giommi 2002). In the sample identified by us, the redshift was deter-

Table 3. Positional Information

Name (1)	RASSBSC Position		NVSS Position		Optical Position	
	RA (J2000) (2)	DEC (J2000) (3)	RA (J2000) (4)	DEC (J2000) (5)	RA (J2000) (6)	DEC (J2000) (7)
SHBL J001527.9+353639	00 15 28.3	+35 36 41	00 15 28.0	+35 36 40.6	00 15 27.9	+35 36 39.1
SHBL J003334.2−192133	00 33 34.6	−19 21 29	00 33 34.3	−19 21 33.7	00 33 34.2	−19 21 33.3
SHBL J004208.0+364112	00 42 08.1	+36 41 15	00 42 08.2	+36 41 12.9	00 42 08.0	+36 41 12.9
SHBL J011501.6−340027	01 15 01.3	−34 00 08	01 15 01.8	−34 00 26.4	01 15 01.6	−34 00 27.0
SHBL J011747.0−244333	01 17 46.6	−24 43 29	01 17 46.9	−24 43 35.0	01 17 47.0	−24 43 33.6
SHBL J012657.2+330730	01 26 57.1	+33 07 30	01 26 57.0	+33 07 27.3	01 26 57.2	+33 07 30.5
SHBL J013632.5+390559	01 36 32.8	+39 05 56	01 36 32.4	+39 05 59.2	01 36 32.5	+39 05 59.6
SHBL J020412.8−333342	02 04 13.6	−33 33 45	02 04 13.2	−33 33 33.9	02 04 12.8	−33 33 42.5
SHBL J031633.7−221611	03 16 34.6	−22 16 12	03 16 33.9	−22 16 11.5	03 16 33.7	−22 16 11.5
SHBL J032350.7+071737	03 23 50.4	+07 17 46	03 23 51.0	+07 17 39.2	03 23 50.7	+07 17 37.0
SHBL J040324.5−242950	04 03 24.0	−24 29 31	04 03 24.6	−24 29 46.6	04 03 24.5	−24 29 50.2
SHBL J041112.2−394143	04 11 12.1	−39 41 30	04 11 11.2	−39 41 42.7	04 11 12.2	−39 41 43.8
SHBL J044127.4+150456	04 41 27.8	+15 04 54	04 41 27.4	+15 04 54.8	04 41 27.4	+15 04 56.0
SHBL J044230.1−001830	04 42 29.8	−00 18 23	04 42 30.0	−00 18 31.1	04 42 30.1	−00 18 30.7
SHBL J050335.3−111507	05 03 35.5	−11 15 04	05 03 35.5	−11 15 06.1	05 03 35.3	−11 15 07.8
SHBL J050939.8−251403	05 09 40.0	−25 13 56	05 09 40.4	−25 14 02.2	05 09 39.8	−25 14 03.0
SHBL J060714.3−251859	06 07 14.2	−25 18 55	06 07 14.3	−25 18 59.6	06 07 14.3	−25 18 59.0
SHBL J062149.6−341149	06 21 49.9	−34 11 40	06 21 49.6	−34 11 54.2	06 21 49.6	−34 11 49.8
SHBL J075124.9+173051	07 51 24.3	+17 30 43	07 51 25.1	+17 30 50.6	07 51 24.9	+17 30 51.0
SHBL J075324.6+292132	07 53 22.3	+29 21 54	07 53 24.3	+29 21 30.8	07 53 24.6	+29 21 32.0
SHBL J092401.1+053345	09 24 01.1	+05 33 50	09 24 01.2	+05 33 42.7	09 24 01.0	+05 33 45.1
SHBL J094355.5−070951	09 43 55.3	−07 09 43	09 43 55.5	−07 09 52.5	09 43 55.5	−07 09 51.2
SHBL J095224.0+750213	09 52 25.8	+75 02 16	09 52 23.7	+75 02 13.2	09 52 24.0	+75 02 13.2
SHBL J095805.9−031740	09 58 06.4	−03 17 29	09 58 06.1	−03 17 38.3	09 58 05.9	−03 17 40.1
SHBL J101015.9−311908	10 10 15.9	−31 19 09	10 10 15.9	−31 19 06.5	10 10 15.9	−31 19 08.6
SHBL J102243.8−011302	10 22 44.2	−01 12 57	10 22 43.8	−01 13 01.8	10 22 43.8	−01 13 02.5
SHBL J104651.4−253545	10 46 51.9	−25 35 46	10 46 51.4	−25 35 47.4	10 46 51.4	−25 35 45.2
SHBL J111939.5−304720	11 19 41.0	−30 46 52	11 19 39.5	−30 47 23.4	11 19 39.5	−30 47 20.2
SHBL J113444.5−172902	11 34 43.5	−17 28 53	11 34 44.5	−17 29 04.0	11 34 44.5	−17 29 02.6
SHBL J113755.4−171042	11 37 55.3	−17 10 34	11 37 55.2	−17 10 30.9	11 37 55.4	−17 10 42.8
SHBL J114535.1−034001	11 45 35.8	−03 39 47	11 45 35.1	−03 39 59.2	11 45 35.1	−03 40 01.4
SHBL J123417.1−385635	12 34 16.9	−38 56 37	12 34 17.4	−38 56 37.8	12 34 17.1	−38 56 35.0
SHBL J123511.0−140322	12 35 11.1	−14 03 32	12 35 10.7	−14 03 23.6	12 35 11.0	−14 03 22.6
SHBL J124149.3−145558	12 41 49.8	−14 55 58	12 41 49.3	−14 55 59.0	12 41 49.3	−14 55 58.0
SHBL J125015.5+315559	12 50 15.0	+31 56 04	12 50 15.7	+31 56 04.0	12 50 15.5	+31 55 59.0
SHBL J125341.1−393159	12 53 41.2	−39 32 00	12 53 41.3	−39 31 59.8	12 53 41.1	−39 31 59.5
SHBL J140630.1−393509	14 06 30.3	−39 35 08	14 06 30.3	−39 35 10.4	14 06 30.1	−39 35 09.3
SHBL J140630.2+123620	14 06 30.0	+12 36 32	14 06 30.0	+12 36 21.1	14 06 30.2	+12 36 20.4
SHBL J140659.2+164207	14 06 59.1	+16 42 04	14 06 59.2	+16 42 09.3	14 06 59.2	+16 42 07.2
SHBL J142739.5−252102	14 27 40.6	−25 21 06	14 27 39.0	−25 20 54.4	14 27 39.5	−25 21 02.0
SHBL J143917.4+393243	14 39 17.7	+39 32 48	14 39 17.4	+39 32 42.4	14 39 17.4	+39 32 43.8
SHBL J144506.3−032612	14 45 05.8	−03 26 13	14 45 06.3	−03 26 13.5	14 45 06.3	−03 26 12.4
SHBL J150340.6−154113	15 03 42.9	−15 41 07	15 03 40.6	−15 41 17.8	15 03 40.6	−15 41 13.9
SHBL J150637.0−054004	15 06 36.4	−05 40 10	15 06 37.0	−05 40 06.5	15 06 37.0	−05 40 04.7
SHBL J151041.0+333504	15 10 40.8	+33 35 15	15 10 42.0	+33 35 08.7	15 10 41.0	+33 35 04.6
SHBL J151618.6−152343	15 16 18.6	−15 23 47	15 16 18.2	−15 23 44.0	15 16 18.6	−15 23 43.0
SHBL J153311.3+185428	15 33 11.7	+18 54 27	15 33 11.5	+18 54 28.8	15 33 11.3	+18 54 28.5
SHBL J161204.6−043815	16 12 04.3	−04 38 16	16 12 04.9	−04 38 19.2	16 12 04.6	−04 38 15.9
SHBL J161632.9+375602	16 16 33.3	+37 55 58	16 16 32.9	+37 55 58.0	16 16 32.9	+37 56 02.7
SHBL J163658.4−124837	16 36 58.7	−12 48 38	16 36 58.4	−12 48 36.6	16 36 58.4	−12 48 37.3
SHBL J174702.3+493801	17 47 02.0	+49 38 03	17 47 02.5	+49 38 03.1	17 47 02.3	+49 38 01.7
SHBL J175615.9+552217	17 56 15.4	+55 22 17	17 56 15.9	+55 22 17.7	17 56 15.9	+55 22 17.7
SHBL J184822.3+653657	18 48 22.6	+65 37 00	18 48 22.7	+65 37 02.1	18 48 22.3	+65 36 57.3

mined based on emission lines only for 8 objects (Appendix B). For most sources (41 objects) we have used the absorption features typical of ellipticals, the strongest of which are summarized in Table 5. In a considerable fraction of our objects (36% or 27/76 objects), however, we observe only a featureless spectrum for which no reliable redshift determination is possible. This fraction reduces to 23% (39/169 objects), if we consider

the entire sample of HBLs (150 sources, Paper II) and emission-line AGN (19 sources, see Paper II).

In order to still be able to conduct meaningful cosmological studies with our sample, we have developed a method of determining lower limits on the redshift of sources without recognizable absorption features. The simulations of Landt, Padovani, & Giommi (2002) of low-redshift BL Lac

Table 3. Positional Information – *continued*

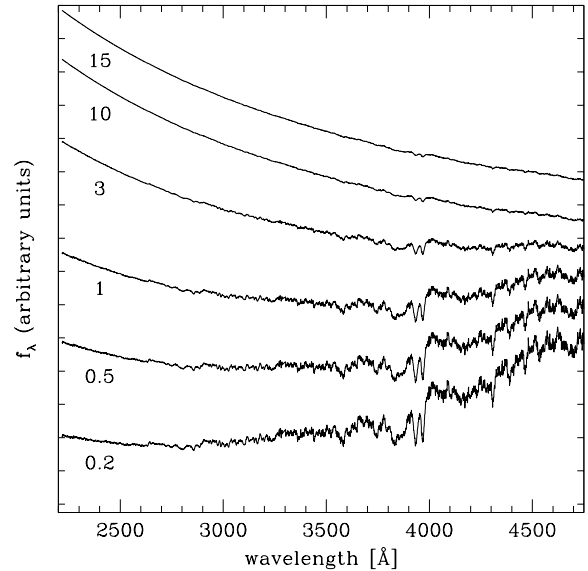
Name	RASSBSC Position		NVSS Position		Optical Position	
	RA (J2000)	DEC (J2000)	RA (J2000)	DEC (J2000)	RA (J2000)	DEC (J2000)
(1)	(2)	(3)	(4)	(5)	(6)	(7)
SHBL J203844.8–263633	20 38 45.0	–26 36 25	20 38 45.1	–26 36 31.7	20 38 44.8	–26 36 33.9
SHBL J204735.8–290859	20 47 37.0	–29 09 01	20 47 36.1	–29 08 57.3	20 47 35.8	–29 08 59.5
SHBL J204921.7+003926	20 49 21.6	–00 39 29	20 49 21.9	–00 39 32.9	20 49 21.7	–00 39 26.9
SHBL J205242.7+081038	20 52 42.5	+08 10 39	20 52 42.9	+08 10 37.4	20 52 42.7	+08 10 38.2
SHBL J213135.4–091523	21 31 35.5	–09 15 25	21 31 35.4	–09 15 22.8	21 31 35.4	–09 15 23.5
SHBL J213151.3–251558	21 31 51.7	–25 16 01	21 31 51.5	–25 15 58.7	21 31 51.3	–25 15 58.8
SHBL J213852.5–205348	21 38 52.8	–20 53 54	21 38 52.8	–20 53 45.3	21 38 52.5	–20 53 48.6
SHBL J222253.8–175321	22 22 53.8	–17 53 17	22 22 54.1	–17 53 24.0	22 22 53.8	–17 53 21.1
SHBL J224910.7–130002	22 49 11.0	–13 00 05	22 49 11.0	–12 59 57.4	22 49 10.7	–13 00 02.8
SHBL J225147.3–320614	22 51 46.8	–32 06 14	22 51 47.5	–32 06 17.0	22 51 47.3	–32 06 14.5
SHBL J230436.8+370507	23 04 37.1	+37 05 06	23 04 36.6	+37 05 07.3	23 04 36.8	+37 05 07.0
SHBL J230722.0–120518	23 07 22.5	–12 05 20	23 07 22.0	–12 05 18.5	23 07 22.0	–12 05 18.1
SHBL J231028.0–371909	23 10 26.9	–37 19 26	23 10 28.2	–37 19 08.5	23 10 28.0	–37 19 09.0
SHBL J234333.8+344004	23 43 32.4	+34 39 57	23 43 33.8	+34 40 00.8	23 43 33.8	+34 40 04.4
SHBL J235023.2–243603	23 50 23.6	–24 35 52	23 50 23.4	–24 36 05.4	23 50 23.2	–24 36 03.6
1RXS J023727.6–26302	02 37 27.6	–26 30 20.0	02 37 27.0	–26 30 27.0	02 37 27.9	–26 30 25.0
1RXS J123802.1+36164	12 38 02.5	+36 16 39.0	12 38 02.1	+36 16 43.0	12 38 02.4	+36 16 39.0
1RXS J130350.5–39503	13 03 50.6	–39 50 53.0	13 03 50.5	–39 50 35.0	13 03 50.6	–39 50 43.0
1RXS J133950.5+15593	13 39 50.3	+15 59 26.0	13 39 50.5	+15 59 32.0	13 39 50.2	+15 59 30.0
1RXS J170817.7–03493	17 08 18.0	–03 49 16.0	17 08 17.7	–03 49 37.0	17 08 17.9	–03 49 16.0
1RXS J182042.7+38171	18 20 43.6	+38 17 01.0	18 20 42.7	+38 17 11.0	18 20 43.5	+38 17 00
1RXS J212516.7–25553	21 25 16.3	–25 55 26.0	21 25 16.7	–25 55 30.0	21 25 16.1	–25 55 30.0
1RXS J222944.5–27553	22 29 45.2	–27 55 36.0	22 29 44.5	–27 55 38.0	22 29 45.2	–27 55 36.0

Table 5. Absorption features typical of ellipticals

Absorption Feature	λ (Å)
FeII	2402
BL	2538
FeII	2609
MgII	2800
MgI	2852
FeI	3000
BL	3096
BL	3580
Ca H&K	3934&3968
G band	4300
H β	4862
MgIb	5174
NaD	5891

spectra (see their Fig. 1) show that BL Lacs are expected to become featureless for jet/galaxy ratios ≥ 10 (defined at 5500 Å). However, the absorption features of ellipticals present at larger rest-frame wavelengths (i.e., redward of the Ca H&K break) are considerably stronger than the ones found at smaller rest-frame wavelengths (see Fig. 2), which means that the situation will be different for high-redshift BL Lacs. For these we expect the spectrum to become featureless at even smaller jet/galaxy ratios.

To determine this value we extended the simulations of Landt, Padovani, & Giommi (2002) to smaller rest-frame wavelengths. Our results are shown in Fig. 2 representative of a jet of optical spectral slope $\alpha = 1$. As soon as the Ca H&K break moves out of the “useful” optical window (i.e., lies at observed wavelengths ≥ 6500 Å, corresponding to redshifts of $z \geq 0.65$, where prominent telluric absorption bands dominate), a redshift determination based on absorption features is expected to be already impossible for sources with jet/galaxy ratios ≥ 1 . Therefore, a featureless, power-law like spectrum indicates that

**Fig. 2.** Simulated BL Lac spectra f_λ vs. λ for a jet of optical spectral slope $\alpha = 1$ and of increasing flux relative to the underlying host galaxy. The assumed jet/galaxy ratios (defined at 5500 Å) are from bottom to top: 0.2, 0.5, 1, 3, 10, 15.

either the BL Lac is at low redshift ($z \lesssim 0.65$) and strongly beamed (i.e., its jet/galaxy ratio is high) or it is at high redshifts ($z \gtrsim 0.65$) where it can be both moderately or highly beamed.

A lower limit on the redshift of featureless BL Lacs can then be determined from the estimate of their minimum jet/galaxy ratio using the fact that ellipticals have a rather constant luminosity. The jet/galaxy ratio constrains the apparent magnitude of the host galaxy from the observed total magnitude of the source,

Table 4. Objects properties

Name	$F_{0.1-2.4\text{keV}}$ [erg/cm ² /s]	$F_{20\text{cm}}$ [mJy]	Vmag	$z^{(a)}$	$\alpha_{\text{iii}}^{\text{opt}(b)}$	Ca H&K break ^(c)	S/N	EW ^(e)
(1)	(2)	(3)	(4)	(5)	(6)	(7)	(8)	(9)
SHBL J001527.9+353639	3.45E-12	11.2	18.2	/	/	/	13	< 5.9
SHBL J003334.2-192133 ^(d)	1.49E-11	18.9	16.1	0.610?	1.04	0	40	< 2.6
SHBL J004208.0+364112 ^(d)	3.68E-12	12	17.9	/	/	/	15	< 5.2
SHBL J011501.9-340027	2.20E-12	6.4	20.1	0.482	1.87	0.14 ± 0.08	15	< 3.1
SHBL J011747.0-244333	3.82E-12	10.3	19	0.279	4.03	0.30 ± 0.05	30	< 2.7
SHBL J012657.2+330730	4.75E-12	7.1	17.5	/	/	/	12	< 6.5
SHBL J013632.5+390559 ^(d)	2.33E-11	60.6	15.4	/	/	/	12	< 6.4
SHBL J020412.8-333342	2.54E-12	6.4	18.6	0.617	1.65	0.04 ± 0.05	27	< 2.9
SHBL J031633.7-221611	2.44E-12	4.4	19	0.228	4.63	0.38 ± 0.08	27	< 2.9
SHBL J032350.7+071737	6.69E-12	4.5	20.3	/	/	/	10	< 7.4
SHBL J040324.5-242950	5.01E-12	7.4	20.1	0.357	2.67	0.09 ± 0.12	25	< 3.5
SHBL J041112.2-394143	4.10E-12	5.3	18.8	/	/	/	12	< 6.5
SHBL J044127.4+150456	3.93E-11	14	19.8	0.109	4.62	0.44 ± 0.28	8	< 8.4
SHBL J044230.1-001830	4.06E-12	4.2	20	0.449	1.51	0.08 ± 0.06	17	< 4.1
SHBL J050335.3-111507	1.29E-11	10.5	17.9	/	/	/	9	< 8.1
SHBL J050939.8-251403	2.13E-12	4.5	20	0.264	1.95	0.07 ± 0.06	30	< 2.7
SHBL J060714.3-251859	4.13E-12	12.2	18.9	0.275	2.70	0.13 ± 0.04	28	< 2.9
SHBL J062149.6-341149	4.47E-12	8.8	18.7	0.529	0.86	0.02 ± 0.04	31	< 2.5
SHBL J075124.9+173051	3.85E-12	10.5	17.4	0.185	?	?	21	< 3.6
SHBL J075324.6+292132	2.78E-12	4.3	18.7	0.161	5.71	0.44 ± 0.14	21	< 3.5
SHBL J092401.1+053345 ^(d)	5.15E-12	7.6	18.4	/	/	/	12	< 6.5
SHBL J094355.5-070951	2.88E-12	7.3	19.9	0.433	2.90	0.19 ± 0.06	22	< 3.1
SHBL J095224.0+750213	4.83E-12	12.4	17.2	0.179	?	?	21	< 3.5
SHBL J095805.9-031740	2.82E-12	7.6	19.6	/	/	/	10	< 7.6
SHBL J101015.9-311908	2.83E-11	74.4	17.3	0.143	1.61	0	41	< 1.8
SHBL J102243.8-011302 ^(d)	1.31E-11	36.3	17.2	/	/	/	15	< 5.0
SHBL J104651.4-253545	4.53E-12	14.3	19.2	0.254	2.27	0.08 ± 0.05	35	< 2.3
SHBL J111939.5-304720	3.72E-12	9.6	19.5	0.412	2.11	0.08 ± 0.05	21	< 3.2
SHBL J113444.5-172902	3.64E-12	5.0	19.7	0.571	1.81	0.02 ± 0.05	30	< 2.5
SHBL J113755.4-171042	4.72E-12	5.3	18.9	0.600	0.66	0	27	< 2.9
SHBL J114535.1-034001	7.96E-12	19.7	18.4	0.167	3.73	0.28 ± 0.12	13	< 5.5
SHBL J123417.1-385635	6.10E-12	7.0	18.0	0.236	4.34	0.31 ± 0.08	23	< 3.4
SHBL J123511.0-140322	2.63E-12	4.2	19.8	0.407	1.66	0.04 ± 0.05	20	< 3.4
SHBL J124149.3-145558 ^(d)	1.81E-11	17.3	17.3	/	/	/	18	< 4.4
SHBL J125015.5+315559	1.88E-12	5.7	19.5	/	/	/	4	< 18.6
SHBL J125341.1-393159	1.96E-11	50.1	18.3	0.179	2.84	0.16 ± 0.09	22	< 3.5
SHBL J140630.1-393509	2.56E-12	6.3	20.6	/	/	/	20	< 3.9
SHBL J140630.2+123620	4.04E-12	8.8	19.8	/	/	/	26	< 3.1
SHBL J140659.2+164207 ^(d)	5.43E-12	8.4	18	/	/	/	16	< 4.9
SHBL J142739.5-252102	4.70E-12	3.7	18.9	0.318	5.12	0.46 ± 0.13	32	< 2.7
SHBL J143917.4+393243 ^(d)	1.79E-11	42.9	16.6	0.344	1.03	0	29	< 2.3
SHBL J144506.3-032612 ^(d)	7.80E-12	21.8	17.4	/	/	/	17	< 4.5
SHBL J150340.6-154113 ^(d)	2.39E-11	5.9	17.5	/	/	/	14	< 5.6
SHBL J150637.0-054004	5.03E-12	15.3	19.5	0.518	1.88	0.05 ± 0.06	28	< 2.6
SHBL J151041.0+333504	4.45E-12	9.1	17.0	0.112	?	?	18	< 3.9
SHBL J151618.6-152343 ^(d)	1.46E-11	8.6	18.7	/	/	/	20	< 4.0
SHBL J153311.3+185428 ^(d)	1.43E-11	23.0	17.7	0.305	1.41	0.015 ± 0.040	22	< 2.8
SHBL J161204.6-043815	4.40E-12	4.3	18.9	/	/	/	11	< 6.8
SHBL J161632.9+375602	1.47E-12	4.6	18.7	0.204	4.18	0.27 ± 0.10	16	< 4.8
SHBL J163658.4-124837	8.74E-12	26.3	20.1	0.246	3.54	0.20 ± 0.03	36	< 2.2
SHBL J174702.3+493801	2.81E-12	7.9	19.9	0.460	2.26	0.13 ± 0.07	20	< 3.6
SHBL J175615.9+552217 ^(d)	1.48E-11	16.9	17.6	/	/	/	12	< 6.4
SHBL J184822.3+653657	4.29E-12	9.7	18.3	0.364	2.86	0.11 ± 0.09	18	< 3.7

which in turn constrains the redshift. For our sample we have assumed jet/galaxy ratios of 1 and 10 and have used the relation $V_{\text{gal}} = 5.10 \cdot \log z + 21.65$ from Browne & Marchã (1993) to estimate redshifts. If the resulting redshift for a jet/galaxy ratio = 10 was higher than $z = 0.65$, we concluded that the source was at high redshifts and that a reasonable lower limit on the redshift could possibly be derived by instead using a jet/galaxy ratio = 1.

This new redshift limit, however, obviously had to be ≥ 0.65 . If this was not the case, we concluded that the Ca H&K break was at observed wavelengths $\gtrsim 6500\text{\AA}$ and chose a conservative lower limit of $z = 0.65$. In practise this means that for sources with total apparent magnitudes $V \lesssim 18.1$, we derived redshift lower limits assuming a jet/galaxy ratio = 10, for sources with $18.1 \lesssim V \lesssim 19.8$ we chose $z = 0.65$, and for fainter sources we

Table 4. Objects Properties – *continued*

Name	$F_{0.1-2.4\text{keV}}$ [erg/cm ² /s]	$F_{20\text{cm}}$ [mJy]	Vmag	$z^{(a)}$	$\alpha_{\text{iii}}^{\text{oi}}^{(b)}$	Ca H&K break ^(c)	S/N	EW ^(e)
(1)	(2)	(3)	(4)	(5)	(6)	(7)	(8)	(9)
SHBL J203844.8–263633	4.73E-12	5.7	18.5	0.437	2.49	0.15 ± 0.07	21	< 3.3
SHBL J204735.8–290859	3.97E-12	10.7	19.3	0.333	2.28	0.09 ± 0.02	33	< 2.6
SHBL J204921.7+003926	4.85E-12	6.0	18.1	0.256	3.25	0.21 ± 0.14	18	< 4.4
SHBL J205242.7+081038	4.90E-12	6.2	19.6	/	/	/	12	< 6.3
SHBL J213135.4–091523 ^(d)	1.58E-11	43.6	16.6	0.449?	0.91	0	26	< 2.7
SHBL J213151.3–251558	6.04E-12	11.0	17.3	/	/	/	18	< 4.2
SHBL J213852.5–205348 ^(d)	1.33E-11	11.5	17.9	0.290	1.22	0	21	< 3.9
SHBL J222253.8–175321	2.88E-12	5.7	19.4	0.297	2.10	0.06 ± 0.05	25	< 3.3
SHBL J224910.7–130002 ^(d)	9.73E-12	7.5	18.9	/	/	/	13	< 5.9
SHBL J225147.3–320614 ^(d)	3.61E-12	3.6	19.0	/	/	/	19	< 4.0
SHBL J230436.8+370507 ^(d)	1.85E-11	23.1	17.8	/	/	/	11	< 7.2
SHBL J230722.0–120518	2.94E-12	7.3	18.5	/	/	/	14	< 5.4
SHBL J231028.0–371909	1.97E-12	6.3	17.8	/	/	/	21	< 3.8
SHBL J234333.8+344004	1.51E-11	35	20.1	0.366	2.19	0.06 ± 0.05	31	< 2.2
SHBL J235023.2–243603	2.14E-12	6.7	16.5	0.193	5.02	0.40 ± 0.19	24	< 3.1

^(a) uncertain redshifts are marked with a “?”.

^(b) Impossible measure of $\alpha_{\text{iii}}^{\text{oi}}$ (the $[O\ II]\ \lambda 3727$ is located in noise) is marked with a “?”.

^(c) we consider the Ca H&K break to have reached its minimum value of zero when the flux blue-ward of this feature is equal to or larger than the one red-ward. The Ca H&K break located in noise are marked with a “?”.

^(d) sources already classified in literature as BL Lacs (see Paper II).

^(e) 2σ upper limit of observed EW, see text for details.

Table 6. Featureless Sedentary HBL.

Name	Vmag	z [lower limit]	Name	Vmag	z [lower limit]
(1)	(2)	(3)	(1)	(2)	(3)
(our sample)			(literature)		
SHBLJ001527.9+353639	18.3	0.650	SHBLJ005816.8+172310 ^(b)	19.2	/
SHBLJ004208.0+364112	18.0	0.623	SHBLJ014040.7–075848	18.3	0.650
SHBLJ012657.2+330730	17.5	0.497	SHBLJ022716.6+020158	18.2	0.650
SHBLJ013632.5+390559	15.4	0.193	SHBLJ023536.6–293843	17.6	0.520
SHBLJ032350.7+071736 ^(a)	20.3	/	SHBLJ030416.3–283217 ^(c)	19.3	/
SHBLJ041112.2–394143 ^(a)	18.8	/	SHBLJ031422.9+061956	18.0	0.623
SHBLJ050335.3–111507	17.9	0.596	SHBLJ035856.1–305448	18.5	0.650
SHBLJ092401.1+053345	18.4	0.650	SHBLJ042900.1–323640	17.6	0.520
SHBLJ095805.9–031740 ^(a)	19.6	/	SHBLJ044018.5–245933 ^(d)	19.5	/
SHBLJ102243.8–011302	15.5	0.202	SHBLJ112348.9+722958	18.5	0.650
SHBLJ124149.3–145558	17.3	0.455	SHBLJ230634.9–110348 ^(e)	19.2	/
SHBLJ125015.5+315559 ^(a)	19.5	/	SHBLJ235730.0–171805	17.3	0.455
SHBLJ140630.1–393509 ^(a)	19.8	/			
SHBLJ140630.2+123620	20.6	0.874			
SHBLJ140659.2+164207	18.0	0.623			
SHBLJ144506.3–032612	17.4	0.476			
SHBLJ150340.6–154113	17.5	0.497			
SHBLJ151618.6–152343	18.7	0.650			
SHBLJ161204.6–043815 ^(a)	18.9	/			
SHBLJ175615.9+552217	17.6	0.520			
SHBLJ205242.7+081038 ^(a)	19.6	/			
SHBLJ213151.3–251558	17.3	0.455			
SHBLJ224910.7–130002 ^(a)	18.9	/			
SHBLJ225147.3–320614 ^(a)	19.0	/			
SHBLJ230436.8+370507	17.8	0.570			
SHBLJ230722.0–120518	18.6	0.650			
SHBLJ231028.0–371909	17.8	0.570			

(a): low quality spectrum; (b): no published spectrum, Nass et al. (1996); (c): no published spectrum, Londish et al. (2002); (d): no spectrum, Schwöpe et al. (2000); (e): no spectrum, Bauer et al. (2000).

derived redshift lower limits assuming a jet/galaxy ratio = 1. We applied this method only to sources with high S/N (≥ 20), high-resolution spectra (26/39 objects), since only these can be reliably classified as definitely featureless. The standard deviation on the relation of Browne & Marchã (1993) is 0.88 in V (see their Fig. 2). This translates into an error of ~ 0.10 in z . In Table 6 we list the featureless objects of our survey (39). The columns are as follows: (1) Sedentary source name; (2) the visual apparent magnitude estimated from the APM for the northern hemisphere and from COSMOS B_J magnitudes, as explained in Paper I; (3) the lower limit redshift computed with the method explained before.

As can be seen in Fig. 2, the spectral optical slope hardens with increasing jet/galaxy ratio. Unfortunately, the measured slope itself cannot be used to improve on the lower limit on z . Since we do not know z , we do not know the rest-frame wavelength and, as can be seen from Fig. 2, the amount of spectral hardening with increasing jet/galaxy ratio differs along the spectrum.

3.5. Classification

The criteria for the classification of a radio-loud AGN as a BL Lac have been continuously revised since the first definition of this object class by Strittmatter et al. (1972) and most recently by some of us (Landt et al. 2004). The separation of BL Lacs from other types of radio-loud AGN, namely radio galaxies and quasars, is based on two features in their optical spectra: the strength of their emission lines and the Ca H&K break absorption value. The first is used to distinguish two intrinsically different classes of radio-loud AGN (BL Lacs and flat spectrum radio quasars), the second is used to separate strongly and weakly beamed sources. Our criteria for classifying BL Lac objects in this survey, as already mentioned in Paper II, was defined by Marchã et al. (1996) and confirmed later by Landt et al. (2002).

We have made no effort to separate the weakly from the strongly beamed sources based on the value of the Ca H&K break (as suggested by Marchã et al. 1996 and Landt et al. 2002), since we did not want to bias our sample against low-luminosity BL Lacs. However, we discuss the Ca H&K-break value distribution of our sources in more detail in Sect. 4.2.

We have also investigated how the classification method of Landt et al. (2004) applies to our sample. We considered all the 169 sources (150 BL Lac and 19 emission line AGN) in the “HBL zone” (see Paper II) and used the [O III] $\lambda 5007$ –[O II] $\lambda 3727$ rest-frame equivalent width plane (see Fig. 4 of Landt et al. 2004) to separate our sources into weak- and strong-lined AGN.

Landt et al. (2004) present evidence of a bimodal [O III] distribution in radio-loud AGN and define the two classes as sources with *intrinsically* weak- and strong [O III] emission lines, respectively. Of the 19 emission-line AGN in our sample (see Paper II; Table 3), 8 sources have been observed by us, and published equivalent width values for [O II] and [O III] are available for a additional 2 sources, namely 1RXSJ000729.3+02405 (Forster et al. 2001) and 1RXSJ122044.5+69053 (Puchnarewicz et al. 1992). We classify only two emission-line AGN, 1RXSJ122044.5+69053 and 1RXSJ222944.5–27553, as weak-lined AGN. Although no information on emission line equivalent widths could be obtained for the 9/11 sources already known, we are confident that these belong to the class of strong-lined AGN. All of these sources are classified in Bauer et al. (2000) as either Seyfert 1 or Seyfert 1.5, which means that they have strong broad emission lines, a characteristic atypical of weak-lined AGN (Landt et al.

2004). For sources observed by us without emission lines, we derived 2σ non-detection upper limits as described in Section 3.3., and based on these, we can classify all of these objects as weak-lined AGN (assuming the same upper limit for both [O II] and [O III]). We assume that this classification also holds for the sources from the literature without emission lines, since those spectra should have had a similar quality to ours. In summary, following the classification method of Landt et al. (2004), our sample contains 152 weak-lined AGN (which we refer to as BL Lacs) and 17 strong-lined AGN.

3.6. Notes on individual spectra

SHBL J001527.9–353639 We classify this object as BL Lac, but its redshift cannot be determined because of the absence of emission and absorption features.

SHBL J003334.2–192133 This object was already identified as BL Lac by Bauer et al. (2000). We confirm its identification and found a tentative redshift of $z=0.610$.

SHBL J004208.0+364112 This object has already been identified as BL Lac by Bauer et al. (2000). We confirm the identification, but its redshift cannot be determined because of the absence of emission and absorption features.

SHBL J012657.2+330730 We classify this object as BL Lac, but its redshift cannot be determined because of the absence of emission and absorption features.

SHBL J013632.5+390559 This object has already been identified as BL Lac by Wei et al. (1999). We confirm the identification, but its redshift cannot be determined because of the absence of emission and absorption features.

SHBL J032350.7–071737 We classify this object as BL Lac, but its redshift cannot be determined because of the absence of emission and absorption features.

SHBL J041112.2–394143 We classify this object as BL Lac, but its redshift cannot be determined because of the absence of emission and absorption features.

SHBL J050335.3–111507 We classify this object as BL Lac, but its redshift cannot be determined because of the absence of emission and absorption features.

SHBL J075124.9+173051 This object was identified as Seyfert 2 by Wei et al. (1999) with redshift $z=0.185$. We confirm its redshift but classify it as BL Lac, as its optical spectrum does not show emission lines. The Ca H&K break for this object is located in noise, so its measurement is impossible.

SHBL J092401.1+053345 This object has already been identified as BL Lac candidate by Bauer et al. (2000). We confirm the identification of BL Lac, but its redshift cannot be determined because of the absence of emission and absorption features.

SHBL J095224.0+750213 This object was identified as an early type galaxy by Bauer et al. (2000) with redshift $z=0.181$. We classify this object as a BL Lac with a redshift of $z=0.179$. The Ca H&K break for this object is located in noise so its measurement is impossible.

SHBL J095805.9–031740 We classify this object as BL Lac, but its redshift cannot be determined because of the absence of emission and absorption features.

SHBL J102243.8–011302 This object has already been identified as BL Lac by Bauer et al. (2000). We confirm the identification, but its redshift cannot be determined because of the absence of emission and absorption features.

SHBL J114535.1–034001 It was classified as cluster of galaxies ($z=0.167$) by Schwobe et al. (2000); since its X-ray emission is not extended we observed it in order to investigate if this object could be a BL Lac in a cluster. From our spectrum we classify it

as a BL Lac and confirm the redshift published by Schwöpe et al. (2000).

SHBL J124149.3–145558 This object has already been identified as BL Lac by Padovani & Giommi (1995b). We confirm the identification, but its redshift cannot be determined because of the absence of emission and absorption features.

SHBL J125015.5+315559 We classify this object as BL Lac. It was observed under non-photometric conditions and is characterized by a low S/N (see Table 6).

SHBL J140630.1–393509 We classify this object as BL Lac, but its redshift cannot be determined because of the absence of emission and absorption features.

SHBL J140630.2+123620 We classify this object as BL Lac, but its redshift cannot be determined because of the absence of emission and absorption features.

SHBL J140659.2+164207 This object has already been identified as BL Lac by Bauer et al. (2000). We confirm the identification, but its redshift cannot be determined because of the absence of emission and absorption features.

SHBL J143917.4+393243 This object has already been identified as BL Lac by Bauer et al. (2000). We confirm its identification and we also found its redshift ($z = 0.344$).

SHBL J144506.3–032612 This object has already been identified as BL Lac by Bauer et al. (2000). We confirm the identification, but its redshift cannot be determined because of the absence of emission and absorption features.

SHBL J150340.6–154113 This object has already been identified as BL Lac by Bauer et al. (2000). We confirm the identification, but its redshift cannot be determined because of the absence of emission and absorption features.

SHBL J151041.0+333504 We classify this object as a BL Lac with redshift $z=0.112$. After our observation in 1999, Schwöpe et al. (2000) classified this object as BL Lac with $z=0.113$, thus confirming our identification.

SHBL J151618.6–152343 This object has already been identified as BL Lac by Bauer et al. (2000). We confirm the identification, but its redshift cannot be determined because of the absence of emission and absorption features.

SHBL J153311.3+185428 This object has already been identified as BL Lac by Bauer et al. (2000). We confirm its identification and we found also its redshift ($z = 0.305$).

SHBL J161204.6–043815 We classify this object as BL Lac, but its redshift cannot be determined because of the absence of emission and absorption features.

SHBL J175615.9+552217 This object has already been identified as BL Lac by Bauer et al. (2000). We confirm the identification, but its redshift cannot be determined because of the absence of emission and absorption features.

SHBL J205242.7+081038 We classify this object as BL Lac, but its redshift cannot be determined because of the absence of emission and absorption features.

SHBL J213135.4–091523 This object has already been identified as BL Lac by Bauer et al. (2000). We confirm its identification and found a tentative redshift of $z = 0.449$.

SHBL J213151.3–251558 We classify this object as BL Lac, but its redshift cannot be determined because of the absence of emission and absorption features.

SHBL J213852.5–205348 This object was classified as candidate BL Lac by Bauer et al. (2000); we confirm its identification and found its redshift ($z = 0.290$).

SHBL J224910.7–130002 This object has already been identified as BL Lac by Bauer et al. (2000). We confirm the identification, but its redshift cannot be determined because of the absence of emission and absorption features.

SHBL J225147.3–320614 This object has already been identified as BL Lac by Bauer et al. (2000). We confirm the identification, but its redshift cannot be determined because of the absence of emission and absorption features.

SHBL J230436.8+370507 This object has already been identified as BL Lac by Cao et al. (1999). We confirm the identification, but its redshift cannot be determined because of the absence of emission and absorption features.

SHBL J230722.0–120518 We classify this object as BL Lac, but its redshift cannot be determined because of the absence of emission and absorption features.

SHBL J231028.0–371909 We classify this object as BL Lac, but its redshift cannot be determined because of the absence of emission and absorption features.

SHBL J235023.2–243603 It was classified as cluster of galaxies ($z=0.193$) by Collins & Mann (1998); since its X-ray emission is not extended, we observed it in order to investigate if this object could be BL Lacs in cluster. From our spectrum we classify it as a BL Lac and confirm the redshift published by Collins & Mann (1998).

4. Sample properties

The full Sedentary HBL sample includes 150 objects and is 100% spectroscopically identified. Redshift have been obtained for 111 objects (74% of the total sample).

4.1. Redshift distribution

The sedentary survey redshift distribution has been de-convolved with the appropriate sky coverage. Each bin represents $\sum 1/\text{Area}(f_x)$ for all the sources in that bin, where $\text{Area}(f_x)$ is the area accessible at its X-ray flux, divided by the total surface density of sources (Landt et al. 2001).

We compared the sedentary survey fractional redshift distribution (see Fig. 3) with various distributions from other BL Lac surveys, namely the complete DXRBS BL Lac sample (Padovani et al. 2007), the 1 Jy (Stickel et al. 1991; Stickel & Kühr 1994; Stocke & Rector 1997), and the EMSS (Rector et al. 2000) samples. The DXRBS and EMSS redshift distributions have been de-convolved with the appropriate sky coverage. Five EMSS redshifts are uncertain, while four 1 Jy redshifts are lower limits (Fig. 3). Five additional 1 Jy sources have a 0.2 lower limit on their redshift based on non-detection of their host galaxies on the optical images (Stickel et al. 1991). Note that the fraction of BL Lacs with redshift information ranges from 93% and 86% for the EMSS and 1 Jy samples, respectively, to 74% and 71% for the sedentary and the DXRBS, respectively.

The mean redshift for the four BL Lac samples is $\langle z \rangle = 0.32$ for the sedentary, $\langle z \rangle = 0.26$ for the DXRBS, $\langle z \rangle = 0.46$ for the EMSS, and $\langle z \rangle = 0.63$ (including lower limits) for the 1 Jy. The sedentary, DXRBS and EMSS samples are peaked at $z = 0.3$, $z = 0.2$ and $z = 0.3 - 0.4$, respectively, and neither sample includes a significant number of $z > 0.8$ objects ($\sim 1\%$ in the sedentary, $\sim 9\%$ in the EMSS, and $\sim 23\%$ in the DXRBS). By comparison, the 1 Jy BL Lacs have a somewhat surprising flat redshift distribution out to nearly $z = 1.5$, with 10/32 1 Jy BL Lacs at $z > 0.8$ and 5 at $z > 1$.

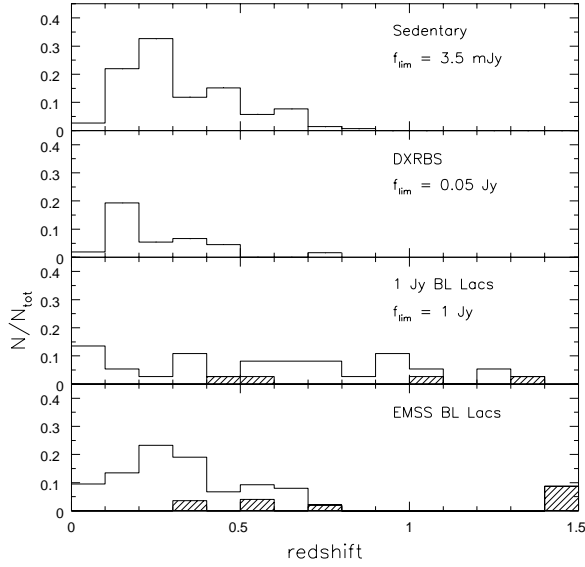


Fig. 3. Fractional redshift distribution for the 111 sedentary, 17 DXRBS, 32 1 Jy, and 38 EMSS BL Lacs. The sedentary, DXRBS, and EMSS distributions have been de-convolved with the appropriate sky coverages. The hatched areas represent lower limits (1 Jy) and uncertain values (EMSS). See text for details.

4.2. The Ca H&K break distribution

Figure 4 shows the Ca H&K break distribution of those HBL (61) from the sedentary survey for which we could take measurements from the literature or from our spectroscopic identifications.

Landt et al. (2002) showed that the Ca H&K break value of low-luminosity, radio-loud AGN is a suitable statistical orientation indicator and can be used to roughly separate the strongly from the weakly beamed sources. This feature is on average ~ 0.5 in normal non-active ellipticals (Dressler & Shectman 1987) and is decreased by the beamed non-thermal jet emission in blazars. We measured the Ca H&K break value for our sources (in spectra plotted as f_λ versus λ) and list these in Table 4. The error represents the 1σ limit and was computed based on the S/N blue ward and red ward of the feature.

Most of sedentary objects have Ca H&K break = 0 or below 0.25. This property was expected, since our sample is constituted by a particular class of BL Lacs, the HBLs, characterized by a synchrotron emission peak located at high energies (UV/X-ray energy band) for which the dilution of host galaxies optical light is very high.

4.3. Optical slopes Vs. radio luminosities

In Fig. 5 we have plotted the optical spectral slopes between the rest frame frequencies of [O II] and [O III] (α_{OII}^{OIII}) of 41 sedentary objects (38 sources with spectra observed by us, 2 sources with spectra from the Sloan Digital Sky Survey (2001) and 1 object from the DXRBS, Landt et al. 2001) versus their radio luminosity (L_r) at 1.4GHz using different symbols for Ca H&K break values in the ranges $C \leq 0.05$, $0.05 < C < 0.25$, and $C \geq 0.25$. The remaining 3 objects with redshift observed by us were excluded from this sample because their Ca H&K break is located in noisy parts of the spectra making its measurement impossible.

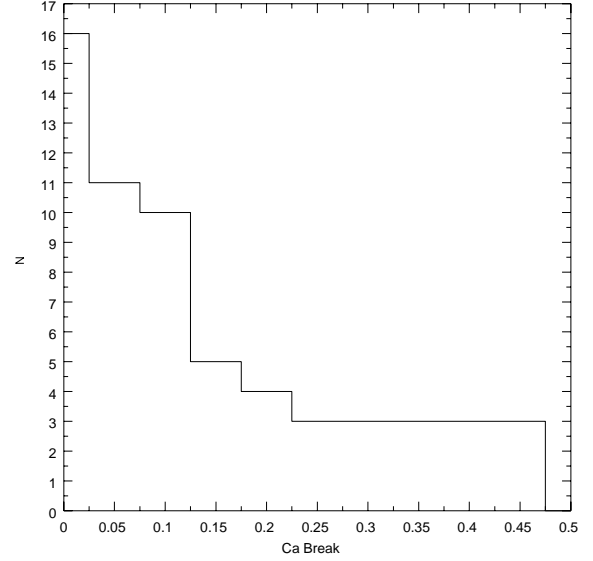


Fig. 4. Ca H&K break distribution of 61 sources from sedentary survey (from literature and from our spectroscopic campaign)

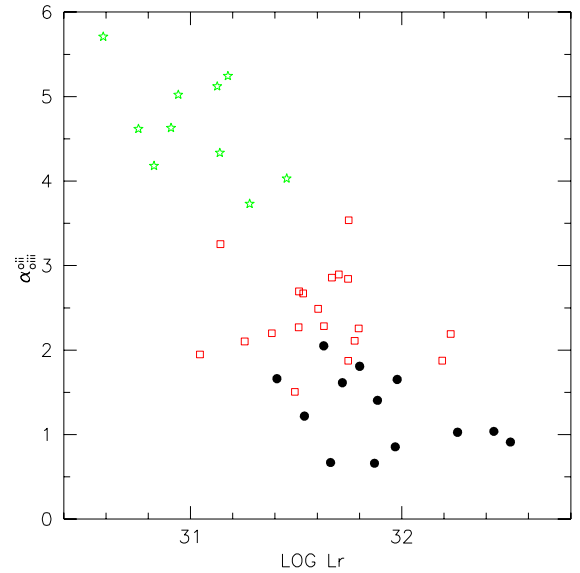


Fig. 5. Optical spectral slopes (α_{OII}^{OIII}) for 38 sedentary objects versus their 1.4 GHz radio luminosity (L_r). Different symbols indicate Ca H&K break values in the ranges $C \leq 0.05$ (filled circles), $0.05 < C < 0.25$ (open squares), and $C \geq 0.25$ (stars).

Landt et al. (2002) showed that the Ca H&K break value decreases with increasing jet powers, concluding that the Ca H&K break value of BL Lacs and radio galaxies is a suitable indicator of orientation. We indeed find that this also applies to the sedentary survey. As Fig. 5 shows, there is a correlation between α_{OII}^{OIII} and L_r , reflecting the fact that for more intrinsically powerful and/or beamed sources (in the radio band), i.e. objects with stronger and/or more beamed non thermal emission, the optical light is dominated by the jet and is therefore characterized by a harder spectrum.

5. Summary and conclusions

We have presented the results of a dedicated optical spectroscopic campaign of the multi-frequency sedentary survey, a flux-limited and statistically well-defined sample of 150 high-energy peaked BL Lacertae objects. Our program, carried out with the ESO 3.6m, the KPNO 4m, and the TNG optical telescopes, led to the spectroscopic identification of *all* sources in the sample.

In this paper we have presented optical spectra for 76 sources, 50 of which are new BL Lac objects, 18 are sources previously known to be BL Lacs but without redshift determination, and 8 are broad emission-line AGNs. We determined 36 redshifts out of the 50 new BL Lacs and 5 new redshifts for the previously known objects. The redshift distribution of the complete sample is presented and compared with that of other BL Lacs samples. For 26 sources without recognizable absorption features, we calculated lower limits to the redshift using a method based on simulated optical spectra with different ratios between jet and galaxy emission.

For a subsample of 38 object with high-quality spectra, we presented the measured Ca H&K break values, and find a correlation between the optical spectral slope, the 1.4 GHz radio luminosity, and the Ca H&K break, indicating that for powerful/beamed sources the optical light is dominated by the non-thermal emission from the jet.

The main cosmological properties, such as the luminosity function and the cosmological evolution of the sample, are studied in detail in Giommi et al. (2007).

Acknowledgements

This work is partly based on optical spectroscopy observations performed at the European Southern Observatory, La Silla, Chile, (Proposals ESO n. 67.B-0222(A), 71.B-0582(A), and 71.B-0582(B)), Telescopio Nazionale Galileo, La Palma, Canary Islands (proposals AOT5/02A, AOT6/02B, AOT7/03A), and Kitt Peak National Observatory. We acknowledge ESO, TNG and KPNO personnel for their assistance during the observing runs. This research has also made use of data taken from the NASA/IPAC Extragalactic Database (NED) and the ESO on-line Digitized Sky Survey on-line services.

References

- Bade, N., Beckmann, V., Douglas, N. G., et al. 1998, A&A, 334, 459
 Bauer, F., Condon, J., Thuan, T., & Broderick, J. 2000, ApJS, 129, 547
 Beckmann, V. 2000, PhD thesis, Hamburg University, <http://www.sub.uni-hamburg.de/disse/330/vbdiss.html>
 Beckmann, V., Engels, D., Bade, N., & Wucknitz, O. 2003, A&A, 401, 927
 Browne, I. W. A. & Marchã, M. J. M. 1993, MNRAS, 261, 795
 Cao, L., Wey, J.-Y., & Hu, J.-Y. 1999, A&AS, 135, 243
 Collins, C. A. & Mann, R. G. 1998, MNRAS, 297, 128
 Condon, J. J., Cotton, W. D., Greisen, E. W., et al. 1998, AJ, 115, 1693
 Dressler, A. & Shectman, S. A. 1987, AJ, 94, 899
 Forster, K., Green, P., Aldcroft, T., et al. 2001, ApJS, 134, 35
 Ghisellini, G. & Maraschi, L. 1989, ApJ, 340, 181
 Giommi, P., Menna, M. T., & Padovani, P. 1999, MNRAS, 310, 465
 Giommi, P. & Padovani, P. 1994, MNRAS, 268, L51
 Giommi, P., Perri, M., Piranomonte, S., & Padovani, P. 2007, in preparation
 Giommi, P., Piranomonte, S., Perri, M., & Padovani, P. 2005, A&A, 434, 385
 Irwin, M., Maddox, S., & McMahon, R. G. 1994, Spectrum, 2, 14
 Landt, H., Padovani, P., & Giommi, P. 2002, MNRAS, 336, 945
 Landt, H., Padovani, P., & Giommi, P. 2004, MNRAS, 351, 83
 Landt, H., Padovani, P., Perlman, E. S., et al. 2001, MNRAS, 323, 757
 Londish, D., Croom, S. M., Boyle, B. J., et al. 2002, MNRAS, 334, 941
 Marchã, M. J. M., Browne, I. W. A., Impey, C. D., & Smith, P. S. 1996, MNRAS, 281, 425
 Morris, S. L., Stocke, J. T., Gioia, I. M., et al. 1991, ApJ, 380, 49

- Nass, P., Bade, N., Kollgaard, R. I., et al. 1996, A&A, 309, 419
 Padovani, P. & Giommi, P. 1995a, ApJ, 444, 567
 Padovani, P. & Giommi, P. 1995b, MNRAS, 277, 1477
 Padovani, P., Giommi, P., Landt, H., & Perlman, E. S. 2007, ArXiv Astrophysics e-prints
 Puchnarewicz, E., Mason, K., Cordova, F., et al. 1992, MNRAS, 256, 589
 Rector, T. A., Stocke, J. T., Perlman, E. S., Morris, S. L., & Gioia, I. M. 2000, AJ, 120, 1626
 Schwöpe, A., Hasinger, G., Lehmann, I., et al. 2000, Astron. Nachr., 321, 1
 Sloan Digital Sky Survey, T. 2001, Early release as obtained in June 5, 2001, Sloan Digital Sky Survey 2001
 Stark, A. A., Gammie, C. F., Wilson, R. W., et al. 1992, ApJS, 79, 77
 Stickel, M., Fried, J. W., Kühr, H., Padovani, P., & Urry, C. M. 1991, ApJ, 374, 431
 Stickel, M. & Kühr, H. 1994, A&AS, 105, 67
 Stocke, J. T. & Rector, T. A. 1997, ApJ, 489, L17
 Strittmatter, P. A., Serkowski, K., Carswell, R., et al. 1972, ApJ, 175, L7
 Urry, C. M., Scarpa, R., O'Dowd, M., et al. 2000, ApJ, 532, 816
 Voges, W., Aschenbach, B., Boller, T., et al. 1999, A&A, 349, 389
 Wei, J., Xu, D., Dong, X., & Hu, J. 1999, A&AS, 139, 575
 Wurtz, R., Stocke, J. T., & Yee, H. K. C. 1996, ApJS, 103, 109
 Yentis, D., Cruddace, R., & Gursky, H. 1992, in Digitised Optical Sky Surveys, ed. H. MacGillivray & E. Thomson (Dordrecht: Kluwer Academic Publishers), 67

Appendix A: 68 sedentary survey spectra

We present here the optical spectra for the 68 Sedentary HBL objects observed during the Sedentary identification campaign from 1999 to 2003 and discussed in this paper.

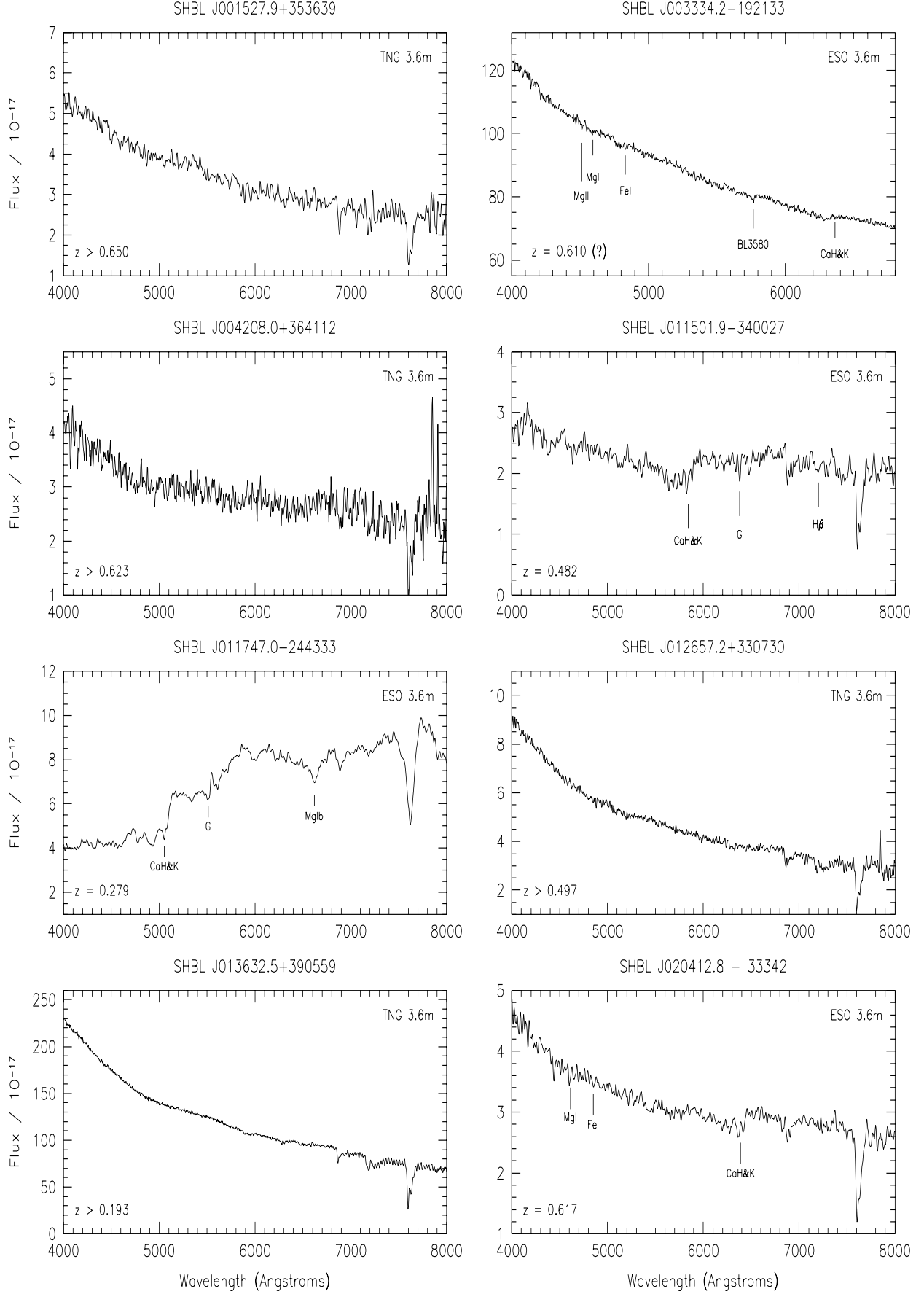
The wavelength in Å is plotted on the x-axis while the y-axis gives the flux f_{λ} in units of 10^{-17} erg cm $^{-2}$ s $^{-1}$ Å $^{-1}$.

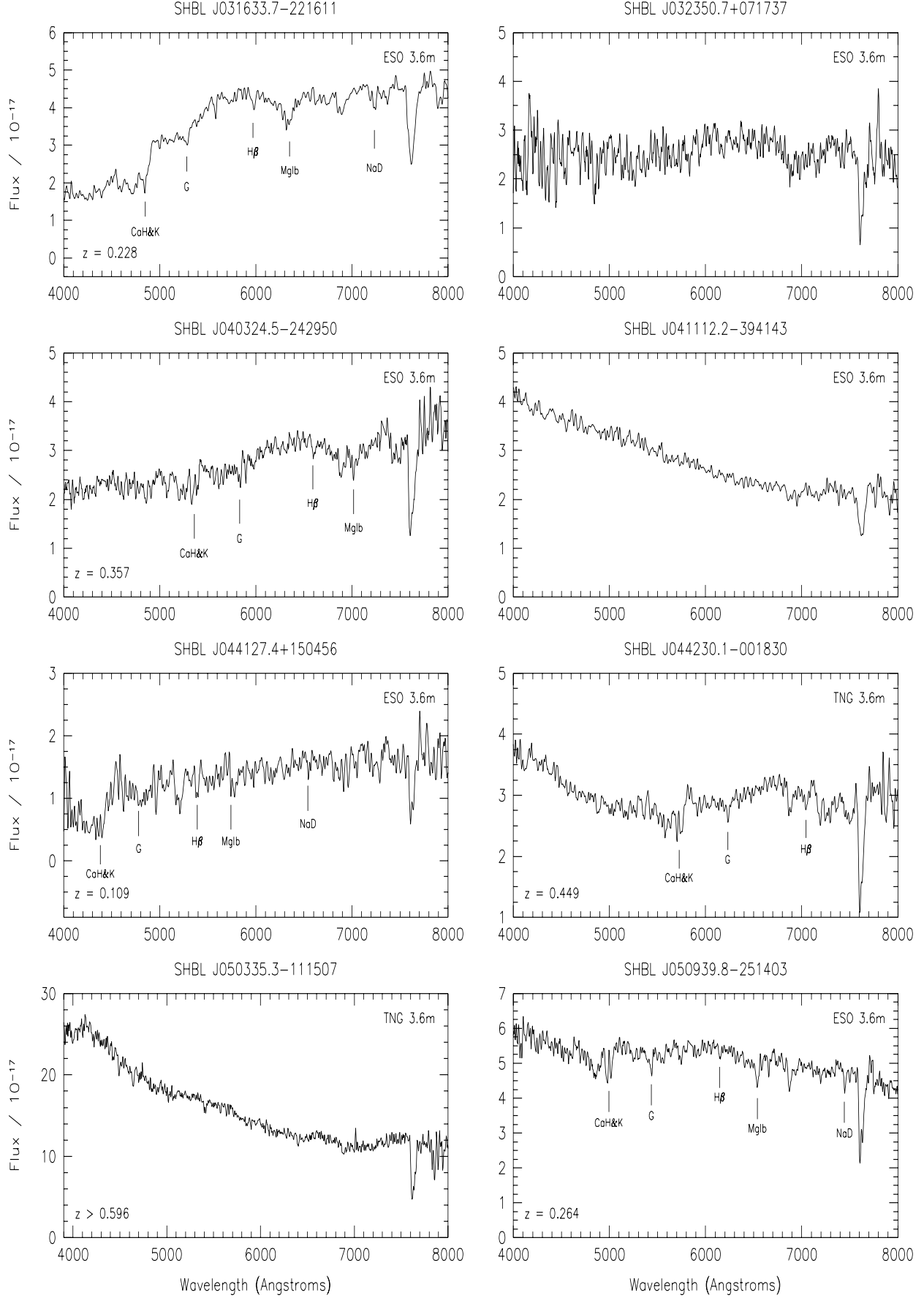
Appendix B: spectra of the 8 AGNs excluded from the sample

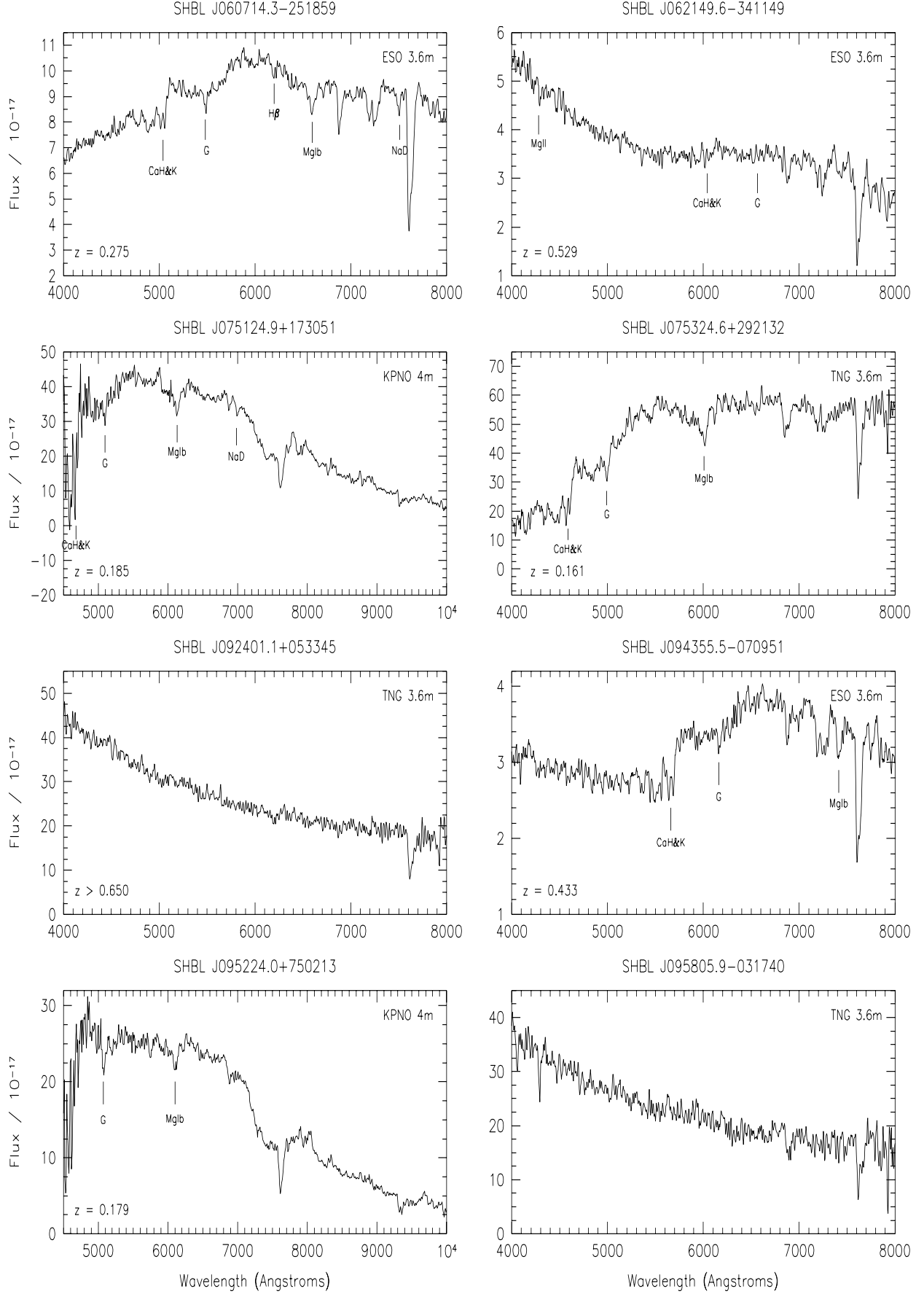
Here we present the optical spectra for the remaining 8 objects observed by us that were broad emission lines AGN and because of that they have been excluded from the sample.

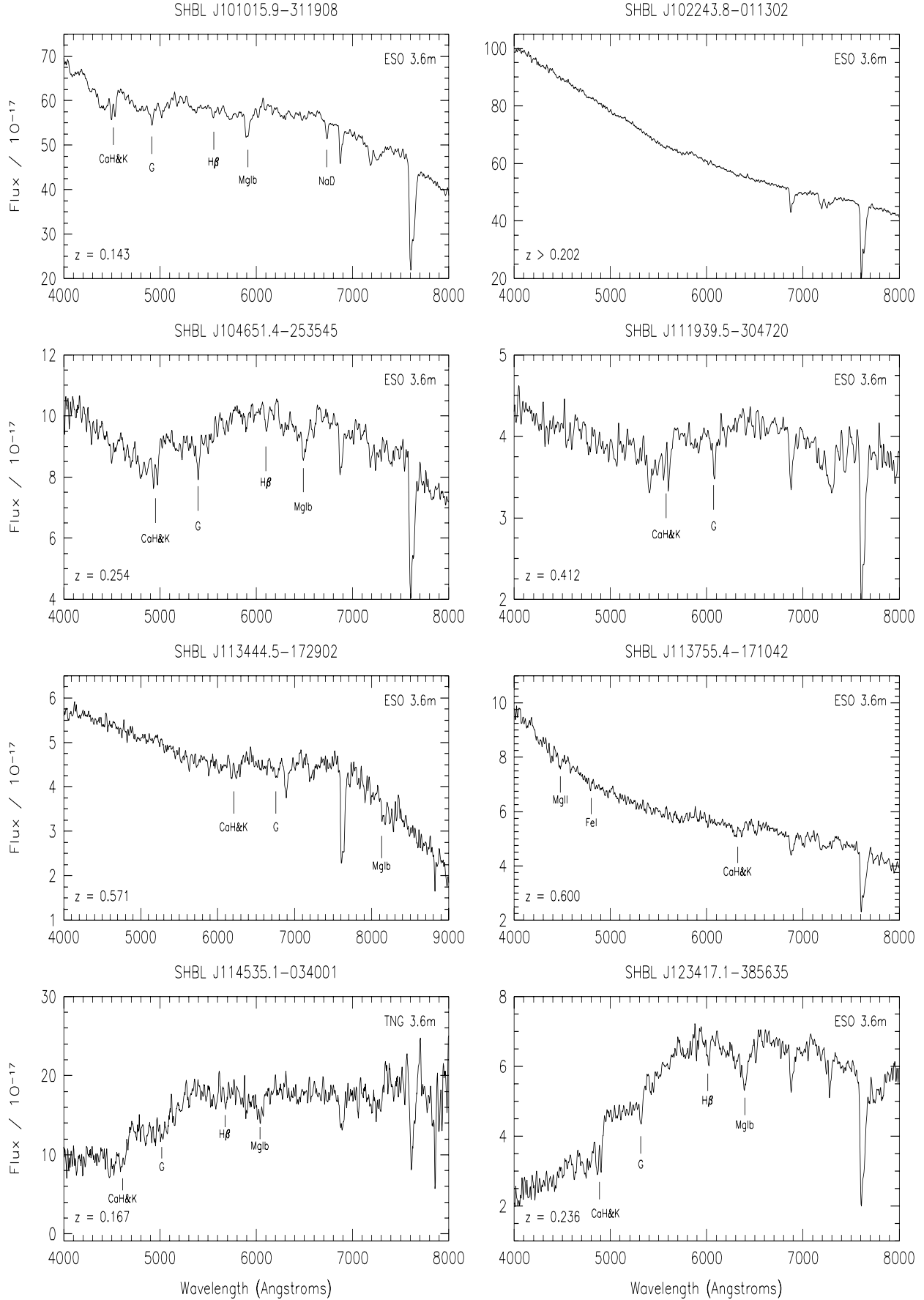
The wavelength in Å is plotted on the x-axis while the y-axis gives the flux f_{λ} in units of 10^{-17} erg cm $^{-2}$ s $^{-1}$ Å $^{-1}$.

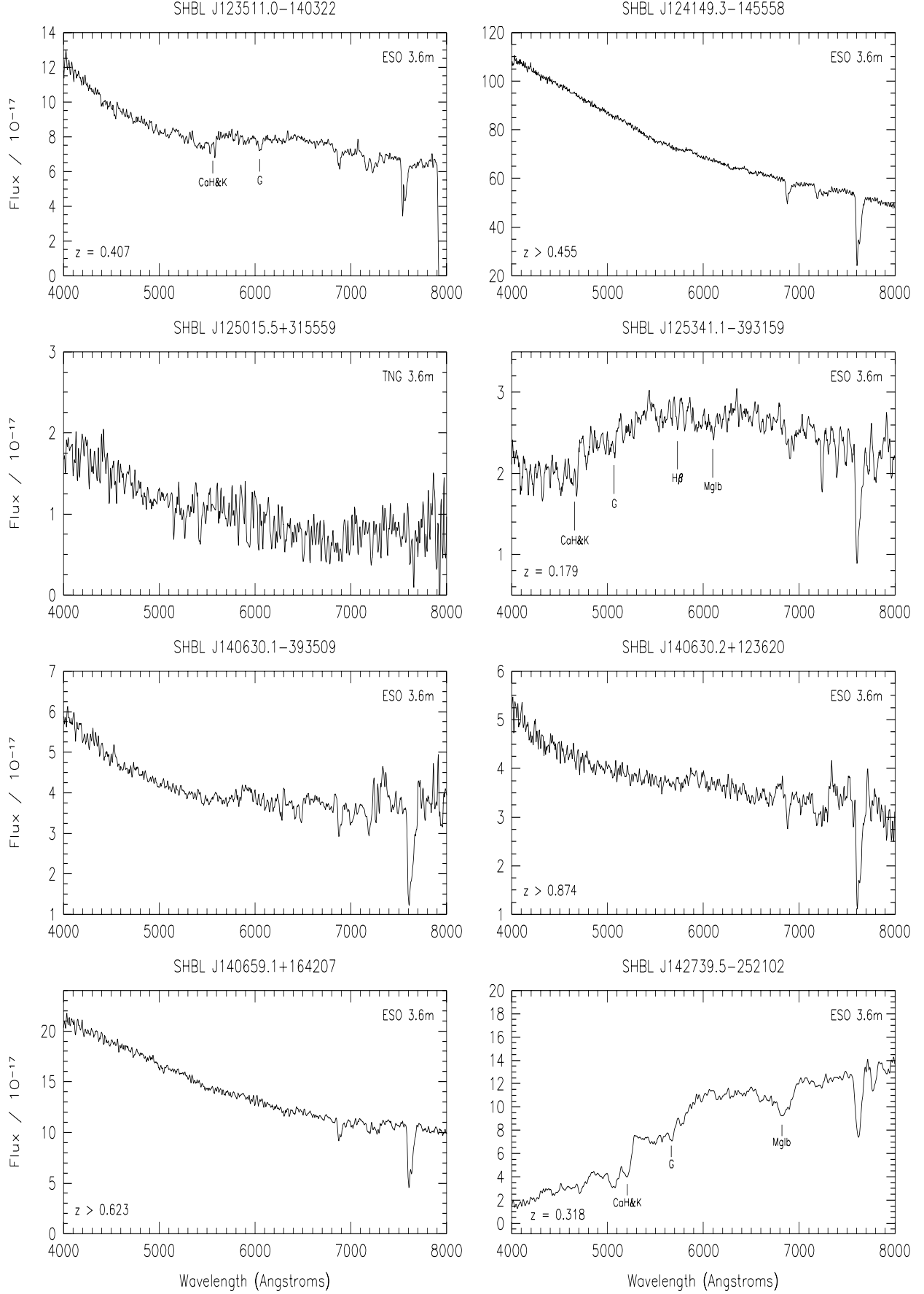
APPENDIX A

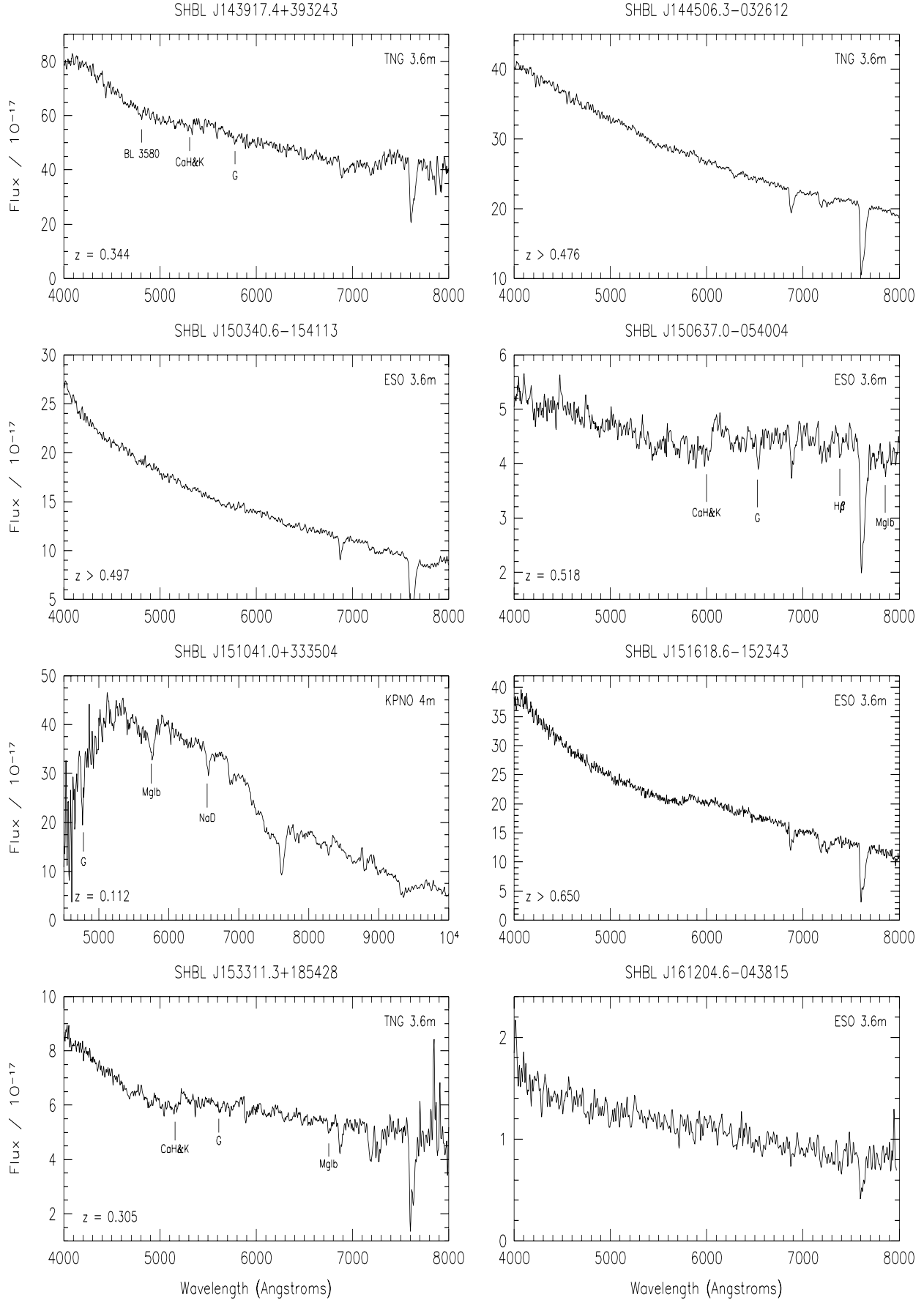


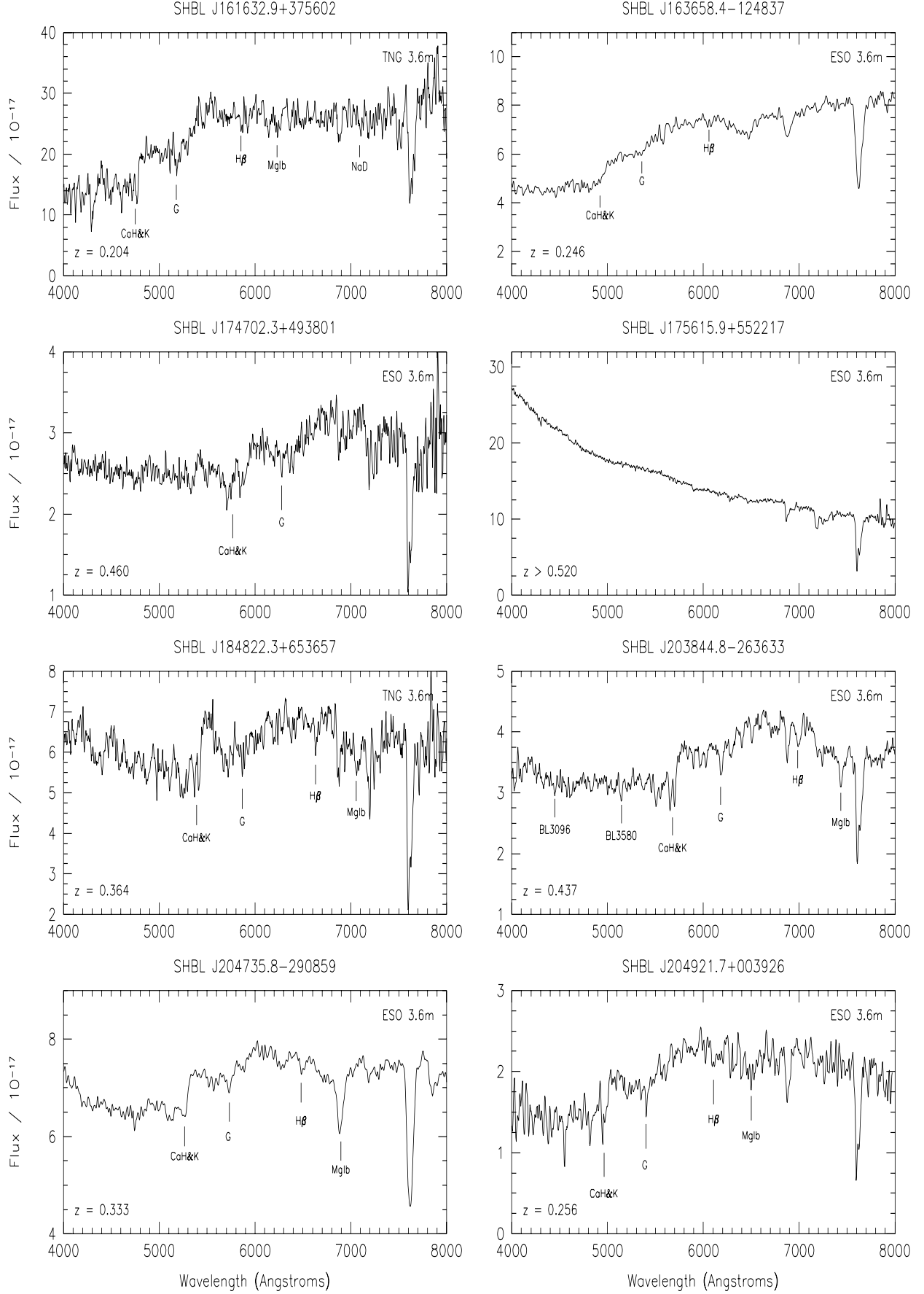


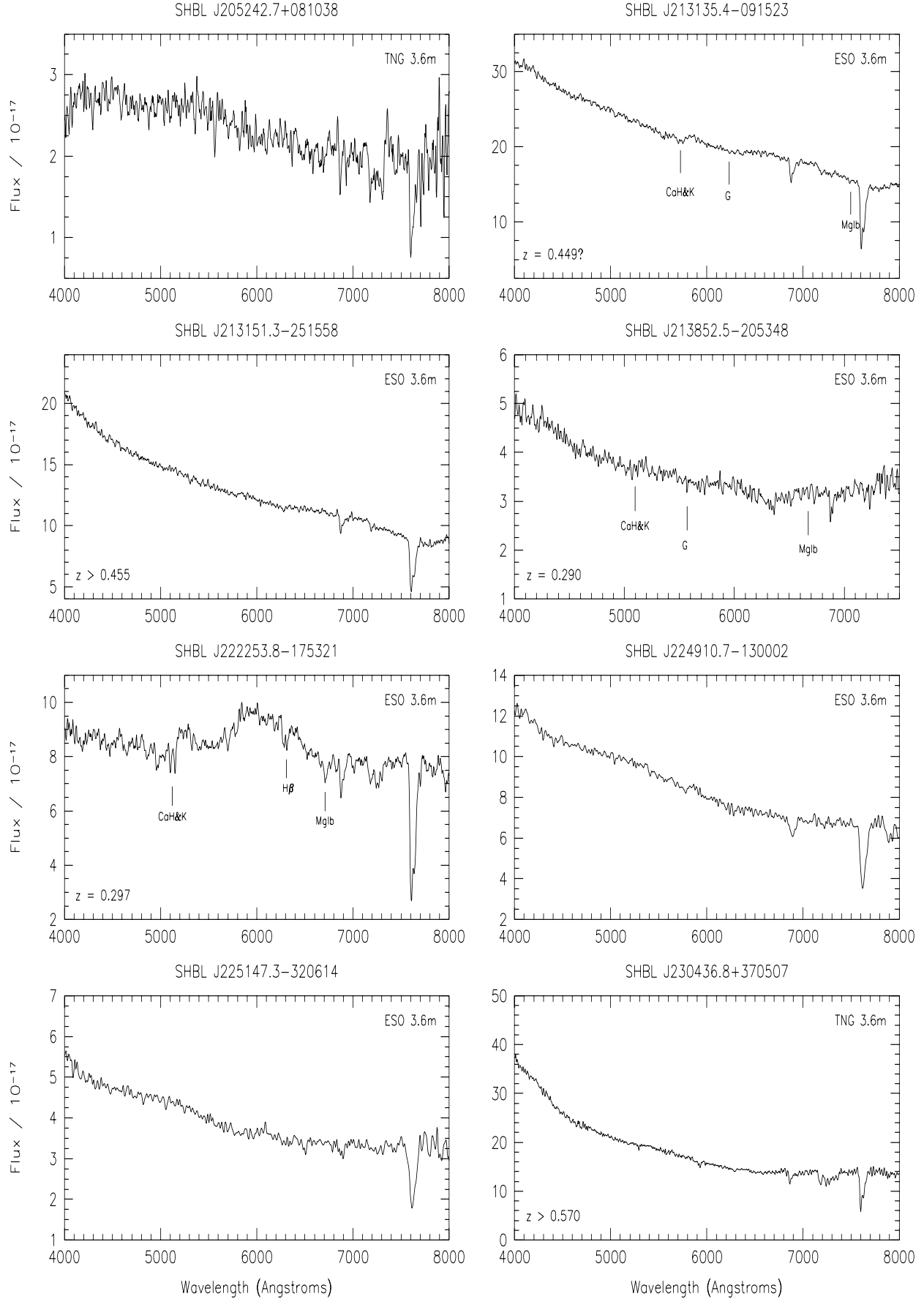


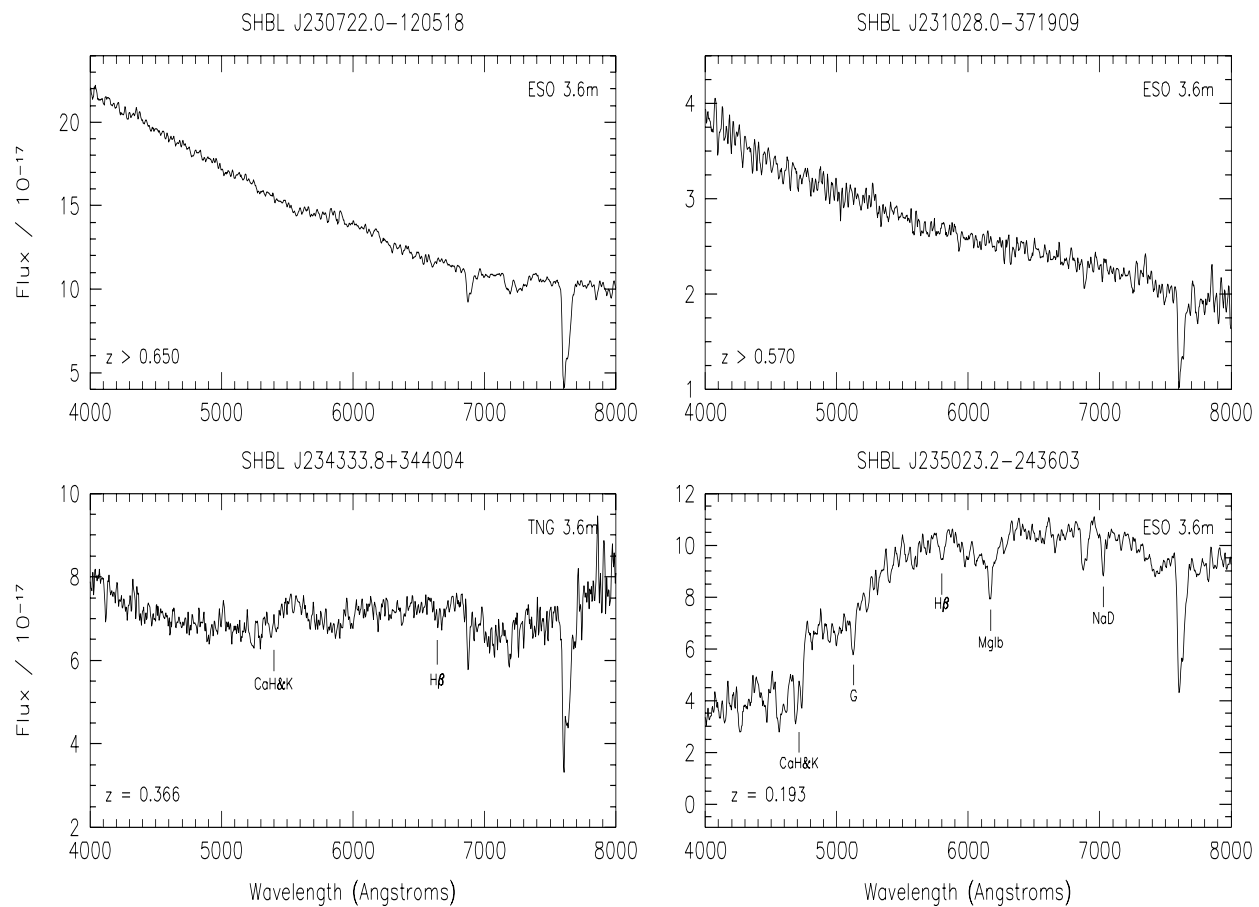












APPENDIX B

